Titan cells formation in *Cryptococcus neoformans* is finely tuned by environmental conditions and modulated by positive and negative genetic regulators

Benjamin Hommel[1,2,3,4,*], Liliane Mukaremera[5,*], Radames J. B. Cordero[6], Carolina Coelho[6], Christopher A. Desjardins[7], Aude Sturny-Leclère[1,2], Guilhem Janbon[8], John R. Perfect[9], James A. Fraser[10], Arturo Casadevall[6], Christina A. Cuomo[7], Françoise Dromer[1,2], Kirsten Nielsen[5], Alexandre Alanio[1,2,3,4,6,*]

[*] These authors participated equally

[1] Institut Pasteur, Molecular Mycology Unit, Département de Mycologie, Paris, France
[2] CNRS UMR2000, Paris, France
[3] Laboratoire de Parasitologie-Mycologie, Hôpital Saint-Louis, Groupe Hospitalier Lariboisière, Saint-Louis, Fernand Widal, Assistance Publique-Hôpitaux de Paris (AP-HP), Paris, France
[4] Université Paris Diderot, Sorbonne Paris Cité, Paris, France
[5] Department of Microbiology and Immunology, University of Minnesota, Minneapolis, Minnesota, USA
[6] Department of Molecular Microbiology and Immunology, Johns Hopkins Bloomberg School of Public Health, Baltimore, MD, USA.
[7] Broad Institute of MIT and Harvard, Cambridge, Massachusetts, USA
[8] Institut Pasteur, Unité Biologie des ARN des Pathogènes Fongiques, Département de Mycologie, Paris, France
[9] Division of Infectious Diseases, Department of Medicine, Duke University Medical Center, [8] Durham, North Carolina, USA
[10] Australian Infectious Diseases Research Centre, The University of Queensland, Brisbane, Queensland, Australia

***Corresponding Author:** Alexandre Alanio, Molecular Mycology unit, Institut Pasteur, 25 rue du Dr Roux 75724 Paris Cedex 15; email: alexandre.alanio@pasteur.fr; Tel: +33140613255; Fax: +33145688420

Abstract

The pathogenic fungus *Cryptococcus neoformans* exhibits morphological changes in cell size during lung infection, producing both typical size 5 to 7 µm cells and large titan cells (> 10 µm and up to 100 µm). We found and optimized *in vitro* conditions that produce titan cells in order to identify the ancestry of titan cells, the environmental determinants, and the key gene regulators of titan cell formation. Titan cells generated *in vitro* harbor the main characteristics of titan cells produced *in vivo* including their large cell size (>10 µm), polyploidy with a single nucleus, large vacuole, dense capsule, and thick cell wall. Here we show titan cells derived from the enlargement of progenitor cells in the population independent of yeast growth rate. Change in the incubation medium, hypoxia, nutrient starvation and low pH were the main factors that trigger titan cell formation, while quorum sensing factors like the initial inoculum concentration, pantothenic acid, and the quorum sensing peptide Qsp1p also impacted titan cell formation. Inhibition of ergosterol, protein and nucleic acid biosynthesis altered titan cell formation, as did serum, phospholipids and anti-capsular antibodies in our settings. We explored genetic factors important for titan cell formation using three approaches. Using H99-derivative strains with natural genetic differences, we showed that titan cell formation was dependent on *LMP1* and *SGF29* genes. By screening a gene deletion collection, we also confirmed that *GPR4/5-RIM101*, and *CAC1* genes were required to generate titan cells and that the *PKR1*, *TSP2*, *USV101* genes negatively regulated titan cell formation. Furthermore, analysis of spontaneous Pkr1 loss-of-function clinical isolates confirmed the important role of the Pkr1 protein as a negative regulator of titan cell formation. Through development of a standardized and robust *in vitro* assay, our results provide new insights into titan cell biogenesis with the identification of multiple important factors/pathways.

57

Author Summary:

Cryptococcus neoformans is a yeast that is capable of morphological change upon interaction with the host. Particularly, in the lungs of infected mice, a subpopulation of yeast enlarges, producing cells up to 100 µm in cell body diameter – referred to as titan cells. Along with their large size, the titan cells have other unique characteristics such as thickened cell wall, dense capsule, polyploidization, large vacuole with peripheral nucleus and cellular organelles. The generation of a large number of such cells outside the lungs of mice has been described but was not reproducible nor standardized. Here we report standardized, reproducible, robust conditions for generation of titan cells and explored the environmental and genetic factors underlying the genesis of these cells. We showed that titan cells were generated upon stresses such as change in the incubation medium, nutrient deprivation, hypoxia and low pH. Using collections of well characterized reference strains and clinical isolates, we validated with our model that the cAMP/PKA/Rim101 pathway is a major genetic determinant of titan cell formation. This study opens the way for a more comprehensive picture of the ontology of morphological changes in *Cryptococcus neoformans* and its impact on pathobiology of this deadly pathogen.

74 **Introduction**

75 The ubiquitous environmental yeast *Cryptococcus neoformans* is a basidiomycetous
76 yeast that has been estimated to cause over 200,000 new cases of meningoencephalitis with
77 greater than 180,000 deaths per year worldwide [1], occurring mostly in
78 immunocompromised individuals with acquired immunodeficiency syndrome (AIDS) [2]. The
79 natural history of most of the cases of this invasive fungal infection proceeds through 3 stages:
80 (i) primary infection via inhalation of desiccated yeasts or basidiospores, with development of
81 sub-clinical pneumonia and spontaneous resolution via granuloma formation; (ii) latency of
82 dormant yeast cells, as demonstrated epidemiologically [3] and biologically [4] and (iii)
83 reactivation and dissemination upon immunosuppression, with meningoencephalitis as the
84 most severe clinical presentation of disease [5]. From the environment to interactions with
85 hosts, the yeasts experience drastic changes that reflect a capacity to rapidly adapt and
86 survive in host tissues and cause disease [4,6–9]. In hosts, *C. neoformans* is exposed to various
87 stresses including high temperature, nutrient deprivation, low pH, hypoxia and high levels of
88 free radicals [10].

89 In response to the host environment, morphological changes are required to survive
90 and cause disease [11]. Specifically, *C. neoformans* alters its morphology and produces
91 enlarged cells referred to as giant or "titan cells" [12,13]. This phenomenon has been observed
92 in animal and insect models of cryptococcosis, as well as in human lung and brain infections
93 [12–16]. Titan cells have increased cell body size, ranging from 10 µm up to 100 µm in diameter
94 [13,17–21] as compared to the 5-7 µm size of typical cells. Studies exploring titan cell biology
95 have revealed that these are: (i) uninucleate polyploid cells [12,13,20]; (ii) possess a large
96 single vacuole; (iii) are surrounded by a thick cell wall [22]; and (iv) have a dense and highly
97 crosslinked capsule [13,17,22]. Titan cells also exhibit increased resistance to various stresses

98 including phagocytosis [21], oxidative and nitrosative stress [20,21], and resistance to the
99 antifungal drug fluconazole [20]. Importantly, titan cell production also enhances
100 dissemination, survival and virulence in a mouse model of infection [19]. Titan cell formation
101 is known to be regulated by the G-protein coupled receptors Gpr5 and Ste3a, that signal
102 through the Gα subunit protein Gpa1 to trigger the cyclic adenosine monophosphate / protein
103 kinase A (cAMP/PKA) signaling pathway [15,20,23–26]. The cAMP/PKA pathway is critical for
104 regulation of other virulence factors in *C. neoformans*, including capsule formation [23,24],
105 notably through its action on the ubiquitin-proteasome pathway [27]. Pka1 is known to be
106 negatively regulated by the protein Pkr1, and *pkr1Δ* mutant strains exhibit enlarged capsule
107 [23]. Further studies show that titan cells formation is increased by high *PKA1* expression or
108 low Pkr1 activity and is decreased by low *PKA1* expression [6]. Downstream of the PKA
109 pathway, Rim101, a major transcription factor that again controls production of many
110 virulence factors, is also necessary for titan cell production [18].

111 To date, studies of titan cell formation have been hindered by an inability to
112 consistently and reproducibly generate large quantities of titan cells *in vitro*. Although several
113 methods have been reported for inducing large cells *in vitro,* there have been persistent
114 problems in easily and consistently implementing these protocols across laboratories [17],
115 presumably because the variables that contribute to titan cell inducing conditions are not well
116 understood.

117 In this study, we identified robust *in vitro* conditions that generate enlarged cells with
118 many of the *in vivo* titan cell characteristics and used this protocol to explore environmental
119 and genetic factors involved in titan cell formation. The genetic determinants of titan cell
120 formation have been investigated through a genotype-phenotype correlation study in H99-
121 derivative laboratory reference strains, through analysis of deletion and complementation in

122 reference strains, and analysis of genetic defects in clinical isolates using whole genome data

123 and complementation.

124 **Results**

125

126 **Titan cells generated *in vitro* had similar characteristics to *in vivo* titan cells**

127 While growth in minimal medium using standard growth conditions has no effect on
128 cell size, we identified growth conditions that stimulated the production of enlarged yeast
129 cells and optimized this experimental protocol, referred to as our *in vitro* protocol, using the
130 reference strain H99O (S1 Fig). Observation of these *in vitro*-generated large cells by
131 microscopy shows many characteristics of titan cells including increased cell body size
132 (diameter >10 µm), refractive cell wall, large central vacuole, and peripheral cell cytoplasm
133 distribution, similar to *in vivo* titan cells (Fig 1A). Our *in vitro* protocol proved to be
134 reproducible with H99O reference strains generating titan cells in three different laboratories
135 throughout the world, although some variability in the overall proportion of titan cells
136 generated was observed (Fig 1B). Specifically, the proportion of titan cells was 39.4%
137 [interquartile range (IQR), [34.1-40.7] in Lab 1, 21.0% [12.5-26.8] in Lab 2 and 29.9% [23.1-
138 48.5] in Lab 3. The distribution of yeast cell body size from the *in vitro* protocol varied from
139 3.7 to 16.3 µm (median 10.2 [8.5-11.5]), whereas *in vivo* it varies from 3.6 to 41.8 µm (median
140 14.8 [11.2-18.45]) with 84% of the yeasts classified as titan cells (Fig 1C).

141 Titan cells differ from typical cells in various characteristics including capsule size
142 budding rate, DNA content, cell wall and capsule structure, and the extent of melanization
143 [12,13,20,22]. Comparison of *in vitro* titan cells (TC) to typical cells (tC) showed a significant
144 increase in capsule size (median 4.8 µm in titan cells vs 2.7 µm in typical cells, $p<0.001$) similar
145 to that observed *in vivo* (median 10.5 µm in titan cells vs 8.0 in typical cells, $p<0.001$, Fig 1D).
146 The capsule thickness of *in vivo* titan cells was increased compared to the *in vitro* titan cells.
147 The budding rate of *in vitro* titan cells was also significantly increased (median 82.5 m per bud)

148 compared to typical cells (median 89.0 m per bud) (p=0.018), whereas it was similar for titan
149 and typical cells produced *in vivo.* Interestingly, overall budding rate was faster *in vivo* than *in*
150 *vitro* cells (68 and 65 m per bud, p<0.001)). The budding rate of both in vivo and in vitro titan
151 cells and typical cells were faster than cells grown in stationary phase (111.5 and 124.5 m per
152 bud in minimal medium (MM) and YPD, respectively) (Fig 1E, S1 Movie, S2 Movie). To analyze
153 DNA content, yeasts obtained at the end of the *in vitro* protocol were stained with propidium
154 iodide (PI) and DNA content of titan (TC, FSC/SSC^{high}) and typical (tC, FSC/SSC^{low}) cells was
155 compared to haploid (H99O) and diploid (AD7-77) strains grown in Sabouraud medium. DNA
156 content was higher in titan (FSC/SSC^{high}) than typical (FSC/SSS^{low}) cells (Fig 1F), with an increase
157 in the proportion of polyploid cells in the titan cell population as observed by a PI fluorescence
158 greater than the diploid control strain (red arrow, Fig 1G). In contrast, the typical cells had the
159 same PI fluorescence pattern as the haploid H99O cells. Similarly, a reverse gating strategy
160 based on PI intensity shows yeasts with the highest PI intensity were large titan cells (red
161 arrows, S2 Fig).

162 Calcofluor white (CFW) staining was used to analyze cell wall chitin content. After
163 multispectral imaging flow cytometry - gating on the titan and typical cell populations under
164 both *in vitro* and *in vivo* conditions (Fig 2A-B) - CFW fluorescence intensity (Fig 2C-D) showed
165 significantly increased fluorescence of titan cells compared to typical cells *in vitro* (322539 ±
166 3072 vs 123062 ± 20727, p<0.0001, Fig 2C) and *in vivo* (144909 ± 38487 vs 27622 ± 7412,
167 p<0.0001, Fig 2D). Cell sorting based on CFW staining and fluorescence microscopy allowed us
168 to validate that cells exhibiting the higher CFW intensity were titan cells (FSC/SSC^{high}, S3B Fig).
169 Measurements of chitin content using fluorescence microscopy also showed significant
170 increases in titan cells compared to typical cells (fluorescence intensity/pixel/cell 87.9 [71.7-
171 107.7] vs 66.5 [51.7-79.4], respectively, p<0.0001, S4A Fig). Chitin levels were also assessed by

172 N-acetylglucosamine (Gluc-NAc) content. Gluc-NAc levels were higher in titan cells (156.3
173 mM/g [153.7-203.7]) than typical cells (97.7 [87.2-119.3]), ($p<0.001$, FigS4B). Furthermore,
174 titan cells exhibited pronounced melanization (S4C Fig), as measured by blackness on the
175 pictures (Fig S4D), compared to typical cells (S5D Fig), with a median of the (max - mean grey
176 intensity per pixel) of 20065 [18785-21887] in titan vs 13067 [9660-15998] in typical cells
177 ($p<0.0001$).

178 Finally, capsule structure was also investigated based on the binding pattern of
179 monoclonal antibodies specific for capsular polysaccharides [28] using multispectral imaging
180 flow cytometry (Fig 2E-F, S5A Fig) and immunofluorescence (S5B Fig). Based on the
181 fluorescence pattern of the 2D10 antibody [29], the algorithm modulation and bright details
182 intensity R7 allowed us to discriminate the distribution of the capsule staining in titan (TC) and
183 typical (tC) cells and showed with almost no overlap between both population *in vitro* (Fig 2E)
184 and *in vivo* populations (Fig 2F). Variability of staining was observed for E1 (IgG1) and 13F1
185 (IgM) antibodies (S5A Fig). No pronounced differences between the capsule structures of titan
186 and typical cells was observed visually during immunofluorescence staining (S5B Fig).

187

188 **Titan cells develop from older cells and produce typical sized daughter cells**

189 To examine temporal changes in cell size induced by our protocol, we measured yeast
190 cell sizes at 0, 4, 8, 16, 24 and 120 h using automated analysis. This automated analysis
191 correlated with manual size measurements (Interclass correlation=0.99) and titan/typical cell
192 classification (Kappa test=0.81±0.07). The median cell size increased during the first 24 h of
193 incubation, starting at 5.7 µm [5.4-6.0] and increasing to 9.7 µm [8.4-11.0] (Fig 3A). The first
194 titan cells were observed at 8 h with a progressive increase in the proportion of titan cells
195 overtime, reaching a plateau by 24 h (Fig 3B).

196 Temporal changes in cell morphology were determined using light microscopy and live
197 cell imaging. Cells with the large vacuole characteristic of titan cells appeared between 4 and
198 8 h (Fig 3C, white arrow). Live cell imaging over 12 h (Fig 3D, S3 Movie) showed that: (i) titan
199 cells swelled from the progenitor typical sized cells and (ii) titan cells divided to produce typical
200 sized daughter cells. CFW staining is known to transfer only partially to daughter cells upon
201 division resulting in lower fluorescence in daughter cells while remaining at a high level in
202 mother cells [4,30]. Pulsed CFW staining was used to further monitor the ancestry of titan and
203 typical cell populations over time using flow cytometry (Fig 3E). The initial CFW stained
204 population (0 h) consisted of typical cells (FSC^{low}) with high CFW fluorescence intensity (black
205 density lines). At 24 h, two populations were observed. The titan cell population (FSC^{high}) had
206 high CFW fluorescence intensity (black arrow), indicating these cells were generated by the
207 swelling of typical sized cells in the original culture. The second population consisted of typical
208 cells (white arrow, FSC^{low}) with low calcofluor fluorescence, consistent with newly formed
209 daughter cells (Fig 3E, right panel). Combined, these data show that the titan cells derived
210 from the initial inoculated cells and daughter cells are typical sized.
211
212 **Generation of titan cells *in vitro* was influenced by environmental conditions**
213 We tested several parameters affecting steps 2 and 3 of our protocol described in S1
214 Fig and identified parameters that significantly influence titan cell generation, as measured by
215 cell size distribution and proportion of titan cells. The first parameter we tested was the
216 growth medium and transition between different growth media (Fig 4A). Initial culture in YPD
217 (step 2) then transfer to MM (step 3) resulted in the highest median cell size at 9.1 µm [6.9-
218 11.1]. Initial culture MM followed by transfer to MM produced fewer titan cells, 25.5%
219 (118/463) vs 39.5% (182/461), although the titan cells tended to be larger with cell body

220 diameters over 20 µm. Light exposure during step 3 also increased both median cell size and
221 proportion of titan cells (Fig 4B). In the light, median cell size was 9.4 µm [7.3-11.4] vs 8.4 µm
222 [7.1-9.9] in the dark, with a titan cell proportion of 41.6% (983/2362) vs 24.3% (1072/4399),
223 respectively (Fig 4B). Incubation temperature at 30°C at step 3 increased cell size distribution
224 compared to 37°C (9.4 µm [7.3-11.4] vs 7.0 µm [6.2-8.2]) as well as the proportion of titan
225 cells (41.6% (983/2362) vs 8.1% (297/3652)) (Fig 4C). The pH of the minimal medium at step 3
226 also influenced cell size (Fig 4D), with pH=5.5 producing significantly larger cells and
227 proportion of titan cells (9.1 µm [6.9-11.2] and 38.6% titan cells), compared to either lower
228 pH (pH=4: median 5.1 µm [4.4-5.8] (0%)) or higher pH (pH=7: 8.2 µm [7.2-9.4] (16.4%), or
229 pH=8.5: 6.9µm [5.9-7.9] (0.7%)) (Fig 4D). Finally, hypoxia at step 3 also increased median cell
230 size compared to normoxia (7.5 µm [5.9-9.7]), with chemically induced hypoxia yielding higher
231 median cell sizes compared to physically induced hypoxia] (10.1 µm [7.8-12.5] vs 8.9 µm [7.3-
232 10.9, $p<0.0001$) (Fig 4E). The proportion of titan cells in normoxia (14.5% (732/5050) was
233 lower than in chemically induced hypoxia or physically induced hypoxia (63.0% (732/1161)
234 and 38.6% (1264/3004), respectively) ($p<0.0001$).
235
236 **Generation of titan cells *in vitro* is influenced by host derived cues**
237 We then tested hosts factors that could interact *in vivo* with yeast cells in the lung such as
238 anticapsular antibodies, serum and phosphatidylcholine. Both serum and phosphatidylcholine
239 have already been implicated in titan cell formation [13,18,31]. Co-incubation at step 3 with
240 monoclonal antibodies that bind to different epitopes of the capsule inhibited titan cell
241 generation, with a decreased cell size of 7.2 µm [6.1-8.3] for E1 mAb, and 6.8 µm [5.9-7.7] for
242 18B7 mAb compared to the untreated control (8.9 µm [7.1-10.6]) (Fig 5A), and a significantly
243 smaller proportion of titan cells (3.2% (44/1360) with 18B7, 5.3% (67/1273) with E1 compared

244 to 33.1% (327/987) for the untreated control). The addition of fetal calf serum (FCS)
245 significantly decreased median cell size (7.3 µm [6.4-8.1] vs (9.1 µm [7.1-11.1], Fig 5B) and the
246 proportion of titan cells (2.5% (99/3911) vs 38.2% (1234/3228), p<0.0001) compared to
247 control, as did the addition of phosphatidylcholine (PC) (8.0 µm [7.0-9.0] vs 9.0 µm [7.1-11.2]
248 for the median cell size, (Fig 5C) and the proportion of titan cells (14.7% (344/2340) vs 38.2%
249 (1077/2820), p<0.0001).
250 To understand if an alteration in yeast metabolism induced by ergosterol, protein or nucleic
251 acids inhibition affected titan cell formation, we tested the effect of co-incubation of
252 fluconazole (inhibitor of ergosterol synthesis) and flucytosine (inhibitor of nucleic acids
253 formation and transcription) and cycloheximide (translation inhibitor) at step 3. Fluconazole
254 (FLC) exposure resulted in significantly smaller median cell sizes compared to the drug-free
255 control (7.1 µm [6.2-8.3]) at 1 mg/L, 6.8 µm [5.9-7.8] at 2 mg/L, and 6.5 µm [5.6-7.2] at 4 mg/L
256 vs 9.4 µm [7.5-11.3] in the control, Fig 5G) and a significantly smaller proportion of titan cells
257 (5.9% (124/2073) at 1 mg/L, 2.9% (55/1919) at 2 mg/L and 1.0% (19/1877) at 4 mg/L vs 40.9%
258 (877/2146) in the control, p<0.0001, Fig 5D). Flucytosine exposure significantly decreased the
259 mean yeast cell size at all concentrations tested (6.5 µm [5.9-6.9] at 1 mg/L, 6.5 µm [6.1-6.9]
260 at 2.5 mg/L, and 6.4 µm [5.9-6.8] at 5 mg/L compared to control (8.3 µm [6.8-10.3], Fig 5E)
261 with no titan cells observed upon flucytosine exposure. Cycloheximide exposure at 0.1 µg/mL
262 also significantly decreased the mean cell size from 9.0 µm [6.3-12.7] to 6.1 µm [5.5-6.9]
263 (p<0.0001) and the proportion of titan cells from 43.3% (797/1840) to 0.1% (20/1663) (Fig 5F).
264 Of note, the viability of the cells recovered at step 4 after 5 d of drug exposure was unchanged
265 for fluconazole but reduced for flucytosine and cycloheximide (p<0.0001 compared to
266 unexposed, S6 Fig).

267 We also tested if iterative subcultures with or without the presence of active molecules
268 (CFW or fluconazole) affected titan cell formation, assuming that the cell wall and the global
269 metabolism of the sub-cultured progeny would be impaired in the presence of high
270 concentrations of the cell wall toxic drug (CFW) or fluconazole, respectively. We analyzed the
271 impact of repeated sub-culture of the cells prior to step 1 on titan cell production (S7 Fig). Sub-
272 culture on Sabouraud agar eight times (8 Sub) spanning a one-month period significantly
273 decreased the median cell size (8.60 µm [7.02-10.07]) compared to the initial culture (0 Sub)
274 (9.17 [6.99-10.90]) ($p<0.0001$). Addition of CFW to induce cell wall stress during sub-culture
275 (8Sub+CFW) significantly decreased the median cell size (8.03 µm [6.82-9.46]) compared to
276 the 8Sub control. Thus, iterative exposure to fluconazole during sub-culture significantly
277 increased the median yeast cell size to 10.15 µm [8.04-13.23] (8Sub+FLC) compared to the
278 8Sub control ($p<0.001$, S7 Fig).
279
280 **Generation of titan cells *in vitro* is influenced by quorum sensing molecules**
281 Previous studies in a murine pulmonary infection model showed that inoculum
282 concentration can impact titan cell production [12,13]. To explore this phenomenon further,
283 we examined cell size changes in response to different initial concentrations of cells at step 3
284 (Fig 6A). Initial cell concentrations significantly impacted the median cell size of the yeast
285 population ($p<0.0001$), with the highest median cell size observed at 10^6 cells/mL (9.2 [7.3-
286 11.1]) compared to 10^5 cells/mL (6.3 [5.1-8.3]), 10^4 cells/mL (6.2 [5.1-7.9]) and 10^7 cells/mL
287 (5.9 [5.2-6.5]) (Fig 6A). Similarly, the proportion of titan cells was significantly higher at 10^6
288 cells/mL (37.6% (896/2382) compared to 10.3% (279/2716) at 10^4 cells/mL, 14.3% (346/2420)
289 at 10^5 cells/mL and 0% at 10^7 cells/mL (0/2177), $p<0.0001$. Previous study reported that
290 pantothenic acid (PA vitamin B5) is involved in quorum sensing and growth rate in *C.*

291 *neoformans* [32]. The addition of PA had no effect on median cell size (8.35 µm [6.9-10.2] and
292 8.3 µm [6.4-10.8], p=0.8011, Fig 6B), but significantly increased the proportion of titan cells
293 (37.9% (1435/3785) vs 26.9% (983/3650)). In specifically implemented experimental settings,
294 the proportion of titan cells was influenced by the concentration of PA with a significant
295 increase in titan cells at 0.125 µM (56.5 [50.6-61.1] and 12.5 µM (47.6 [35.6-50.3]) (Fig 6D). In
296 parallel, analysis of the growth curves of the yeast showed a significant increase in the
297 doubling time (slope) at ≥0.125 µM of PA (Fig 6E), suggesting a lack of correlation between
298 titan cell formation and growth rate because titan cell formation was completely inhibited at
299 1250 µM of PA while the doubling time increased.
300 Recent studies in *C. neoformans* also implicate the role of the small Qsp1 peptide in quorum
301 sensing [33]. Addition of Qsp1 peptide significantly decreased median cell size from 9.1 µm
302 [7.1-11.2] to 8.5 µm [6.9-10.1] (Fig 6C) and titan cell proportion from 38.4% (1075/2798) to
303 26.6% (915/3439), p<0.0001. Addition of Qsp1 peptide inhibited the formation of titan cells
304 in H99O (Fig 6C) and KN99α (Fig 6F). In the *qsp1Δ*, *pqp1Δ* and *opt1Δ* deletion mutants that
305 cannot produce or import a functional Qsp1 peptide [33], titan cell generation was increased
306 compared to KN99α, confirming the negative regulation of Qsp1 peptide in titan cell formation
307 (Fig 6F). When *qsp1Δ*, *pqp1Δ* were complemented with Qsp1 but not with scrambled Qsp1
308 peptides, titan cell formation was similar (increased titan cell formation) to that of the mutant
309 alone. The complementation of the *opt1Δ* deletion mutant with Qsp1 or scrambled Qsp1 did
310 not rescue the parental phenotype suggesting that the import of Qsp1 is crucial for its action
311 on the yeast cells (Fig 6F).
312
313 ***In vitro* titan cell generation is dependent upon H99 genetic background and requires**
314 **functional *LMP1, SGF29* and *SREBP* genes.**

315 Previous whole genome sequencing studies identified single-nucleotide
316 polymorphisms (SNPs) and insertions/deletions (indels) between H99-derived strains
317 recovered from various laboratories (Table 1) [34]. To determine whether any of these SNPs
318 or indels affected titan cell generation, we tested the H99S, H99W, H99 CMO18, H99L, KN99α
319 strains. H99O produced significantly more titan cells than the other H99-derived strains,
320 p<0.0001 (Fig 7A, S8A-S9 Fig). These H99 derivative strains were also tested for titan cell
321 formation in the lungs of infected mice (S8A-S9 Fig). As with *in vitro* titan cell production, all
322 the H99 derivative strains showed lower levels of titan cell formation *in vivo* when compared
323 to H99O (p<0.0001), with the exception of KN99α that had equivalent titan cell production to
324 H99O (Fig 7A, S8A-S9 Fig).
325 Two genes, *LMP1* and *SGF29*, are dramatically affected by SNPs/indels in the H99 derivatives;
326 *LMP1* has a frameshift deletion (H99W and H99 CMO18) and *SGF29* is deleted (KN99α and
327 H99L) [35]. To determine if these genes are involved in titan cell production, we analyzed
328 *lmp1Δ* and *sgf29Δ* deletion mutants for *in vitro* and *in vivo* titan cell formation (Fig 7 and S8-
329 S9 Fig, respectively). In vitro, the *sgf29Δ* mutant in the H99O background had half the titan
330 cell formation of the H99O wild-type strain [8.1% (49/600) to 4.2% (25/600), p<0.0001]. The
331 *sgf29Δ* mutant in the hypervirulent H99S also manifested no titan cells generation, as did an
332 *lmp1Δ* mutant in this background. Complementation of *LMP1* and *SGF29* in this H99S mutant
333 restored titan cells generation to that found in the parental strain; 1.2% (13/935) and 1.4%
334 (7/600), respectively vs H99S 1.6% (25/1540) (Fig 7B). Importantly, the same trend was
335 observed for *in vivo* titan cell formation*. In vivo,* the *lmp1Δ* H99S mutant produced only 3.5%
336 (21/600) titan cells compared to 14% for H99S (84/600), p<0.0001, and this decrease in titan
337 cell production was restored in the *lmp1Δ:LMP1* H99S strains (9.5% (57/600)) (S8B Fig) .The
338 *sgf29Δ* mutant in the H99O background reduced titan cell formation *in vivo* from 18.8%

339 (113/600) to 9.3% (37/400) (p<0.0001). In H99S, complementation of Sgf29 *(sgf29Δ:SGF29*) in
340 H99S restored titan cell generation to wild-type H99S levels from 5% (30/600) to 19.8%
341 (237/1200) (Fig 7B, S8B Fig) (p<0.0001).
342 SREBP is a gene involved in response to hypoxia, so we tested titan cell formation in the *sre1Δ*
343 mutant. The proportion of titan cells was significantly decreased in the *sre1Δ* mutant at 5.1%
344 (53/920) compared to KN99α [14% (337/2358)] (p<0.0001) (S10 Fig).
345

346 ***In vitro* titan cell generation requires signaling through the Gpr/PKA/Rim101 pathway and**
347 **is dependent on negative regulators**

348 The signal transduction pathway Gpr/PKA/Rim101 regulates titan cell formation *in vivo* [18].
349 Briefly, the G-protein coupled receptor 5 and Ste3a pheromone receptor signal through Gpa1
350 to trigger the cAMP/PKA signaling cascade, ultimately activating the Rim101 transcription
351 factor. This pathway regulates virulence factors such as capsule or melanin [36,37].
352 To determine if this same pathway was critical for titan cell generation *in vitro*, we
353 examined cell enlargement in the *gpr4Δ*, *gpr5Δ*, *gpr4Δ/gpr5Δ, rim101*Δ, and *cac1Δ* mutants
354 and their complemented strains in both the H99 and KN99α genetic backgrounds (Fig 7C-7D,
355 S9 Fig). In the H99O genetic background, Rim101 function was similar to that observed *in vivo*,
356 with little titan cell formation in the *rim101Δ* mutant (1.9% (51/2600)) and full restoration of
357 titan cell production in the complemented strain (9.2% (239/2600) (p<0.0001) (Fig 7C). In
358 KN99α, the *rim101Δ, gpr4Δ/gpr5Δ,* and *cac1Δ* mutants had no titan cell formation, but
359 surprisingly both of the single *gpr4Δ* and *gpr5Δ* mutants also lacked titan cell formation (Fig
360 7D). This is in contract to *in vivo* where titan cell production was rescued by GPR5 alone [18].
361 Taken together, these data suggest that signaling through both Gpr4 and Gpr5 via the
362 cAMP/PKA pathway to Rim101 is required for titan cell production *in vitro*.

363

364 ***In vitro* titan cell formation is regulated by PKR1 in clinical isolates**

365 To determine whether the Gpr/PKA/Rim101 pathway can impact titan cell formation
366 in clinical isolates, we also screened a total of 56 clinical isolates for their ability to produce
367 titan cells. Two isolates (AD2-06a and AD2-02a) produced a more titan cells relative to H99O
368 (ratio of clinical strain/H99O of 2.6±0.3 and 1.4±0.3, respectively). Three additional isolates
369 (AD4-37a, AD1-95a, AD4-43a) produced fewer titan cells than H99O (ratio=0.4±0.3, 0.2±0.1,
370 0.1±0.0, respectively). Titan cell production in the other clinical isolates was close to zero (ratio
371 between 0.1 and 0.01% for five, less than 0.01% for six, and no titan cells at all for the
372 remaining 39 isolates) (Fig 8A).

373 The complete genome sequence was obtained for 41 of the total 68 screened clinical
374 isolates and a phylogenetic tree of these strains and the H99O reference strain shows high
375 genetic diversity including VNI, VNII, VNBII isolates (Fig 8B, Table 2). Compared to H99O, the
376 high titan cells generating strain AD2-06a harbored 31,229 SNPs and was closely related to
377 AD3-55a (31,171 SNPs) and AD3-41a (28,599 SNPs), which were both unable to produce titan
378 cells. A total of 19 genes, including CNAG_00570 (*PKR1*), were disrupted in AD2-06a and not
379 in AD3-55a and AD3-41a (S1 Table). Of note, no common genetic mutation, insertion or
380 deletion has been observed in the 3 strains that produced a significant (>1%) proportion of
381 titan cells (H99O, AD2-06a, AD1-95a) as compared to all the other examined isolates.
382 Duplication of chromosomal regions were observed in the French sequenced clinical isolates
383 (S2 Table) with AD2-06a harboring a large duplication of chromosome 9 (Chr9, region 465 –
384 665kb). To assess whether the Chr9 duplicated region could be responsible for titan cell
385 formation, we explored a larger collection of *C. neoformans* strains with complete genome
386 sequence [38] and discovered five additional clinical isolates (Ug2459, CCTP20, FFV14, WM-

387 148, WM-626) harboring partial duplications on chr9 duplication (S11 Fig). We analyzed titan
388 cell formation in these 5 isolates, but only the Ug2459 strain generated titan cells *in vitro* and
389 only at a low proportion (S11 Fig), suggesting that genes located within in the AD2-06a Chr9
390 duplication are not involved by themselves in titan cell formation.

391 AD2-06a was isolated from the initial cerebrospinal fluid (CSF) sample of an HIV-
392 infected patient at baseline (diagnosis of cryptococcosis). Another isolate, AD2-07, was
393 recovered from the CSF of the same patient after 13 d of amphotericin B treatment. Thus,
394 AD2-06a and AD2-07 are closely related with only 137 different SNPs and 40 indels. AD3-55a
395 is in the same clade and also very similar with 370 different SNPs and 64 indels, although
396 recovered from another patient and in another place (Fig 8B-8C). By contrast, these three
397 isolates differ from H99O by 29,000 SNP and 3,386 indels. AD2-07 and AD3-55a were both
398 unable to produce titan cells (Fig 8A, 8B, 8E), allowing a more fine-scale analysis of SNPs linked
399 to titan cell formation in these closely related strains (Fig 8C). Specifically, AD2-07 produced
400 1.0% (31/3047) titan cells compared to 39.1%, (639/1633) in AD2-06a and 15.2% (304/2001)
401 in H99O ($p<0.0001$). The median cell size of AD2-07 was significantly decreased compared to
402 AD2-06a and H99O (5.9 µm [5.2-6.6] for AD2-07, 8.5 µm [7.0-13.0] for AD2-06a, and 7.7 µm
403 [6.5-9.2] for H99O, $p<0.0001$, S12 Fig).

404 Comparison of the AD2-06a, AD2-07, and AD3-55a genomes identified four genes with
405 loss-of-function mutations in AD2-06a but not in AD2-07 or AD3-55a: CNAG_00570 (PKR1) (Fig
406 8D), CNAG_07475 (hypothetical protein), CNAG_01240 (hypothetical protein) and
407 CNAG_05335 (hypothetical protein). More precisely, AD2-06a had a frameshift mutation at
408 glycine 124 in the CNAG_00570 (*PKR1*) leading to a truncated protein of 138 amino acids (Fig
409 8D). Pkr1 is the cAMP-dependent protein kinase regulatory subunit that interacts with Pka to
410 regulate the phosphorylation activity of Pka. To further explore *PKR1* in clinical isolates, we

411 analyzed additional, previously sequenced, clinical isolates (S3 Table) that harbored mutations
412 leading to Pkr1 truncation (Bt156, Bt58, 8-1, Bt77, Bt117, Ug2462) for titan cell formation [39].
413 Specifically, a frameshift mutation at amino acid 14 introducing a premature stop codon at
414 position 96 for Bt156, as well as stop codons introduced at positions 130 for AD2-06a, 258 for
415 Bt58, 302 for 8-1, 439 for Bt77, 441 for Bt117, and 445 for Ug2462 was observed (Fig 8E, Table
416 3). We hypothesized that the strains with highly impacted/truncated Pkr1 protein would
417 produce more titan cells, similar to the AD2-06a isolate. AD2-06a and Bt156, the strains with
418 the largest truncation, had high levels of titan cell formation with a ratio of 2.8±1.0 for AD2-
419 06a and 1.3±0.6 for Bt156 compared to H99O (Fig 8E), and titan cell proportions and median
420 cell sizes of 39.1% (639/1633) (median 8.5µm [7.0-13.0]) and 17.9% (469/2614) (median
421 7.7µm [6.4-9.4]), respectively (S12 Fig). For the other strains, the ratio, proportion of titan
422 cells, and median size were decreased compared to H99O: 0.2±0.0, 3.6% (89/2464) and 6.9
423 µm [6.0-7.8] for 8-1 strain; 0.2±0.1, 2.9% (110/3834) and 6.5 µm [5.8-7.1] for Bt77; 0.1±0.0
424 0.9% (27/3081) and 6.4 µm [5.7-7.2] for Bt117; and 0.1±0.1, 1.5% (54/3628) 5.4µm [4.7-6.1]
425 for Ug2462, $p<0.0001$) (Fig 8E, S12 Fig).

426 To directly test whether the truncated Pkr1 protein impacted titan cell production in
427 strain AD2-06a, the functional KN99α allele of the *PKR1* gene was introduced into the strain
428 (AD2-06a*:PKR1*) and titan cell formation analyzed. Titan cell production was significantly
429 decreased by complementation ($p<0.0001$) with 44.9% (574/1279) for AD2-06a*:PKR1* as
430 compared to 64.6% (700/1083) for AD2-06a and 23.2% (555/2363) for H99O (Fig 8F).

431 To further explore the function of *PKR1* in titan cell formation, we also tested the ability
432 of *pkr1Δ* in a KN99α background to generate titan cells compared to KN99α, and found that
433 *pkr1Δ* produced more titan cells with a ratio of 4.9±1.6 compared to the parental strain KN99α
434 (Fig 9). The *pkr1Δ* median cell size (8.1 µm [6.7-9.5]) exceeded that of KN99α (6.4 µm [5.5-

435 7.2]) p<0.0001) with a significant increase in the proportion of titan cells at 28.5% (695/2436)
436 for *pkr1Δ* vs 4.6% (121/2614) for KN99α (p<0.0001, Fig 9A). We also analyzed titan cell
437 production in two additional independent *pkr1Δ* and complemented *pkr1Δ:PKR1* strain in the
438 H99 background. The *pkr1Δ-1 and* complemented *pkr1Δ:PKR1-1* gave ratios of 2.9±1.5 and
439 1.8±0.7, respectively, while the *pkr1Δ-2 and* complemented *pkr1Δ:PKR1-2* ratio were 1.9±0.8
440 and 1.4±0.4, respectively, compared to the H99 parental strains (1.0±0.5) (Fig 9B). In both
441 strains, complementation significantly reduced the proportion of titan cells generated
442 (p<0.0001) from 29.8% (685/2493) for *pkr1Δ-1* to 18.8% (593/3217) for *pkr1Δ:PKR1-1*; and
443 from 19.9% (422/2364) for *pkr1Δ-2* to 13.9% (359/2588) for *pkr1Δ:PKR1-2* with H99 at 10.3%
444 (357/3674). We also tested the role of *PKA1* and *PKR1* using the galactose-inducible and
445 glucose-repressible versions of *PKA1* and *PKR1* mutants [6]. In these mutants, when incubated
446 in galactose minimal medium (Fig 9C), the genes are turned on whereas when incubated in
447 glucose minimal medium the genes are turned off (Fig 9D). In galactose minimal medium,
448 P_{GAL7}::PKA1 and P_{GAL7}::PKR1 had titan cell production ratios of 5.6±1.1 and 0.6±0.5 compared
449 to H99, respectively. The proportion of titan cells was significantly increased upon *PKA1*
450 induction [46.9% (794/1724)] and reduced by *PKR1* induction [4.7% (222/5031)] compared
451 with H99 in galactose minimal medium at 14.8% (402/3108) (p<0.0001, Fig 9C). In glucose
452 minimal medium, P_{GAL7}::*PKA1* and P_{GAL7}::*PKR1* had titan cell production ratios of 0.0±0.0 and
453 2.4±1.0, respectively. The proportion of titan cells was significantly decreased upon *PKA1*
454 repression [0.2% (6/4156)] and increased by *PKR1* repression [25.4%(527/2425)] compared
455 with H99 at 10.3% (357/3674) (p<0.0001, Fig 9D).
456 At least 2 other genes (*TSP2*, *USV101*) have been linked to titan cells formation *in vivo* although
457 their role is less clear, so we directly explored their phenotypes in our *in vitro* protocol. To
458 examine the role of tetraspanin 2 (Tsp2) in titan cell formation *in vitro*, we analyzed three

459 independent tetraspanin 2 deletion mutants (*tsp2Δ-1, tsp2Δ-2* and *tsp2Δ-3*) and two
460 complemented mutants (*tsp2Δ-1:TSP2-1* and *tsp2Δ-1:TSP2-2*) for their titan cell formation
461 compared to the wild-type KN99α. Titan cell production was significantly increased in the
462 deletion mutants (23.9% (518/2161) for *tsp2Δ-1,* 55.7% (990/1778) for *tsp2Δ-2,* 44.3%
463 (714/1610) *tsp2Δ-3,* 4.6% (119/2576)) compared to the wild-type and complemented strains
464 (*tsp2Δ-1:TSP2-1,* 5.8% (228/3877) for *tsp2Δ-1:TSP2-2* and 4.9% (173/3472) for KN99α)
465 ($p<0.0001$) (Fig 9E). Similarly, *usv101Δ* median cell size (10.6 µm [8.7-12.7]) was higher than
466 the parental strain KN99α (7.6µm [6.6-8.8]) and the proportion of titan cells was 62.7%
467 (1260/2008) for *usv101Δ* vs 10.5% (238/2262) for KN99α ($p<0.0001$) (S9 Fig).
468 We finally selected additional sequenced clinical isolates that harbored mutations leading to
469 Usv101 or Cac1 truncation. Bt88 showed a truncation of Usv101 and an increased titan cells
470 formation ratio 0.6±0.4 whereas the other isolates belonging to the VNBII lineage harboring a
471 *CAC1* mutation (Bt133 and Bt31, Bt40, Bt89 and Bt105) did not show increased titan cells
472 formation (ratio 0.0±0.0) (S13 Fig).

473 **Discussion**

474 We identified and validated a new protocol allowing robust generation of titan cells *in*
475 *vitro*. This protocol was discovered serendipitously while testing conditions that could induce
476 dormancy in *C. neoformans* [4]. We observed yeast cell enlargement under defined growth
477 conditions, then optimized those conditions for titan cell production. It is important to note
478 that the utility of other published protocols to generate titan cells *in vitro* are hindered by
479 issues with inter-laboratory reproducibility [13,31]. To establish the inter-laboratory
480 transferability of our protocol, we independently tested it in two other laboratories (K. Nielsen
481 and A. Casadevall) and observed that the protocol produced similar results in all laboratories,
482 although slight variations of the materials and equipment used produced subtle variability in
483 the percentage of titan cells generated in the 3 labs. Interestingly, titan cell production *in vitro*
484 was also optimized by Ballou et al. 2017 and Zaragoza et al. 2017, using a different set of
485 growth conditions [40,41]. Exploration of the similarities and differences between these
486 protocols will likely identify the critical environmental conditions that trigger titan cell
487 production *in vivo*.

488 Titan cells obtained *in vitro* exhibited many of the characteristics of *in vivo* titan cells
489 recovered from the lungs of infected mice [17]. Similar to previous work on *in vivo* titan cells,
490 we defined the *in vitro* titan cells as having a cell body size > 10 µm and typical cells with a cell
491 body size ≤ 10 µm [12,13,18,21]. Titan cells generated with our *in vitro* protocol were also
492 polyploids, as previously shown *in vivo* [12,13]. Melanization was increased in *in vitro* titan
493 compared to typical cells. Capsule size was slightly increased in the *in vitro* titan cells
494 compared to typical cells, but this difference was lower than previously shown *in vivo* [12,13].
495 We also demonstrated that, regardless of the capsule size differences between *in vitro* and *in*
496 *vivo* titan cells, the structure of the *in vitro* titan cell capsule was different to that in typical

497 cells, a phenomenon also observed *in vivo* [13,22]. The cell wall was thicker in *in vitro* titan
498 cells compared to typical cells, as previously analyzed *in vivo* [22,31,42]. The increased chitin
499 in the titan cell wall results in a detrimental immune response that exacerbates disease[42].
500 These findings suggest a fundamental difference in titan and typical surface structure that may
501 contribute to reduced titan cell phagocytosis [12,13,21]. These cell surface differences also
502 underscore the complex regulation of these major virulence factors and shows intricate
503 adaptation of *C. neoformans* to both *in vitro* and *in vivo* conditions.

504 Titan cell generation *in vitro* allowed a detailed kinetic analysis that revealed titan cells
505 are formed between 4 and 8 h. Using calcofluor white staining to follow cell fate and cell
506 division [4,30], we showed that titan cells were exclusively derived from cells present in the
507 initial inoculum that evolved progressively toward the titan cell phenotype. In contrast, typical
508 cells were a mixture of cells from the initial inoculum and new cell replication. Titan cell
509 division produced typical sized haploid cells, as shown previously for *in vivo* titan cells [12,13]
510 and confirmed in our study. We published *in vivo* data that validate this observation [4]: using
511 yeasts recovered from the lung of mice at one week after inoculation of *C. neoformans* stained
512 with calcofluor and multispectral imaging flow cytometry, we showed that the Calcofluor^{High}
513 population was associated with yeast cells harboring high cell size parameters compatible with
514 titan cells [4]. *In vitro*, titan cell generation coincided with the appearance of a large vacuole
515 in the yeast cells at 4 and 8 h of incubation. Recent evidence places vacuoles at the center of
516 networks enabling nutrient resources to be degraded, sorted and redistributed [43]. As the
517 vacuole volume occupies much of the total volume of the titan cell body, one can imagine that
518 cell-cycle regulation could be impacted, ultimately leading to polyploidy [42].

519 The fact that our *in vitro* protocol consistently produced titan cells also allowed us to
520 test factors that influenced their appearance. In terms of environmental factors, we showed

521 that titan cell production was influenced by pre-culture medium, initial pH, light exposure,
522 temperature, type of medium and hypoxia. A metabolic switch between YPD (rich medium)
523 pre-culture and minimal medium (poor medium) incubation was a key factor to induce titan
524 cell generation. This switch is a stress that induces many metabolic modifications and has been
525 studied extensively in *Saccharomyces cerevisiae* [44]. Hypoxia is another stress factor
526 encountered by human pathogenic fungi during infection [45], and a strong signal for titan cell
527 production *in vitro*. Oxygen levels in healthy human tissues are 20–70 mmHg (2.5–9% O_2), but
528 can be less than 10 mmHg (~1% O_2) in hypoxic or inflamed tissues or inside granulomas [46].
529 We know from previous work on pulmonary aspergillosis that hypoxia has been observed in
530 infected lungs of mice [47]. Titan cells have been reported in human pulmonary cryptococcosis
531 and well-studied in murine pulmonary infection following inhalation [13,17–21], although
532 they are also observed in mouse lungs after intravenous inoculation of animals [4]. These
533 observations lead us to hypothesize that low oxygen levels in the lungs could be a signal for
534 titan cell formation. A major transcriptional regulator of the fungal hypoxia response is the
535 sterol regulatory element-binding protein (Srebp) [48]. Deletion mutants of the *SREBP* gene
536 (*sre1Δ*) in *C. neoformans* display defects in adaptation to hypoxia, ergosterol synthesis,
537 susceptibility to triazole antifungal drugs and cause a reduction of virulence [48]. Importantly,
538 the *sre1Δ* mutant also showed defects in titan cell production *in vitro*, highlighting the role of
539 hypoxia in titan cell production.

540 Interestingly, quorum sensing is also involved in titan cell production. Indeed, the initial
541 concentration of yeasts in minimal medium dramatically impacted titan cell generation, with
542 10^6 cells/mL being the optimal cell concentration to generate titan cells *in vitro*. No titan cell
543 formation was observed with a starting concentration of 10^7 cells/mL, likely due to rapid
544 consumption of the nutrients preventing metabolic modifications needed to generate titan

545 cells. Alternatively, addition of the quorum Qsp1 peptide [33,49] to wild type cultures (already
546 producing Qsp1) decreased titan cell production, suggesting that Qsp1 negatively regulates
547 titan cell production. Cleavage and internalization of Qsp1 were critical because the *qsp1Δ,*
548 *pqp1Δ*, *opt1Δ* mutants all showed increased titan cell production. Pantothenic acid (vitamin
549 B5) has also been implicated in quorum sensing in *C. neoformans* [29]. Addition of pantothenic
550 acid dramatically increased titan cell formation at concentrations between 0.125 and 12.5 µM.
551 These results demonstrate that intercellular communication is important for titan cell
552 formation and that this sensing process involves cell-cell communication instead of simple
553 nutrient sensing.

554 Induction of titan cells due to the presence of host factors such as temperature,
555 addition of lipids, presence of serum, and antibodies was also tested. The presence of E1 [50]
556 and 18B7 [51] anti-capsular IgG antibodies decreased titan cell production. This decrease
557 could be related to changes in yeast metabolism induced directly by anti-capsular antibodies,
558 as shown previously [52], and provides a new mechanism by which antibodies could alter the
559 course of infection. One could imagine that specific anti-capsular antibodies may not reach
560 cryptococcal cells in the alveolar space at sufficient concentration to impair enlargement. The
561 presence of surfactant protein-D, considered as an opsonin in the lung, could impair antibody
562 fixation [53], thus inhibiting the inhibitory effect of IgG antibodies and allowing titan cell
563 formation in the lung. Interestingly, addition of serum (5% FCS) or L-α-phosphatidylcholine
564 decreased titan cell production, which is different from other protocols for titan cells
565 generation [40,41]. This difference may be because our protocol induces titan cells through
566 parallel or independent pathways to those triggered by serum or lipids. Overall, these results
567 imply the existence of numerous triggers for titan cell formation mediated through

568 independent signaling pathways. How these pathways ultimately interact, both positively and
569 negatively, to regulate titan cell production still needs to be explored.

570 Titan cell production was inhibited by addition of fluconazole, flucytosine and
571 cycloheximide - even at concentrations that or below the MIC of the drug. Fluconazole is
572 known to inhibit the 14-alpha-demethylase (Erg11) involved in ergosterol synthesis, leading
573 to plasma membrane instability and accumulation of toxic precursors [54]. Flucytosine is a
574 base analogue leading to inhibition of DNA replication and protein synthesis [55].
575 Cycloheximide is known to impact protein synthesis through inhibition of translation [27].
576 Thus, titan cell production likely involves an active process requiring protein and nucleic acid
577 production, as well as plasma membrane integrity (normal ergosterol quantity). Conversely,
578 serial passage in the presence of fluconazole increased titan cell production, suggesting
579 compensatory changes in response to fluconazole also impacted titan cell production. These
580 data have profound implications for *in vivo* titan cell production, as prolonged drug therapy
581 could prevent or enhance titan cell formation. In previous studies, exposure of titan cells to
582 fluconazole selected for aneuploidy and drug resistance in the daughter cells [20]. In contrast,
583 our studies show exposure to cell-wall stress, induced by serial passage on CFW agar,
584 decreased titan cell production. In these sub-culture experiments, we did not investigate
585 subsequent genomic or metabolic changes that arise under these stress conditions. Serial sub-
586 culture could have induced genetic rearrangements (aneuploidy, SNPs, indels) or epigenetic
587 variation that altered titan cell production.

588 Our protocol is easy to implement for study of the molecular and genetic mechanisms
589 underlying titan cell generation. Our *in vitro* assay allowed us to identify host, environmental
590 and yeast factors that impact titan cell production. By taking advantage of strains harboring
591 genetic differences and clinically relevant genetic truncations, we were able to assess genetic

592 factors modulating titan cell production. However, these studies also highlight that variability
593 in titan cell formation cannot be completely explained by the acquisition of genetic events,
594 with H99-derivative strains showing diversity in titan cell production that does not fully
595 correlate with genetic modifications. The observation that titan cell formation in KN99α differs
596 *in vitro* (lower than H99O) and *in vivo* (equivalent to H99O) highlights this issue and suggests
597 further strain adaptation that are yet to be characterized.

598 We uncovered new genes involved as positive or negative regulators of titan cell
599 production. Sgf29, is a component of the SAGA complex that binds H3K4me2/3 and recruits
600 histone deacetylases in *S. cerevisae* [56]. The *LMP1* gene is known to be involved in virulence
601 in a mouse model and in mating [34]. We showed here that both genes are positive regulators
602 of titan cell formation, although their mechanism of action remains unclear. We also showed
603 *in vitro* the critical role of the Gpr/PKA/Rim101 pathway in titan cell formation, previously
604 characterized *in vivo* [18]. Gpr5 signals through Gpa1 to trigger the PKA pathway that activates
605 the transcription factor Rim101 [18,36]. In addition, we identified three genes that are
606 negative regulators of titan cell formation, including *PKR1* (known to act as a regulatory
607 subunit in the PKA pathway [23], *TSP2* that encodes a glucose repressor of laccase in *C.*
608 *neoformans* [57], and *USV101* that is a pleiotropic transcription factor in *C. neoformans* known
609 to regulate capsule formation and pathogenesis [58].

610 In *Saccharomyces cerevisiae*, the Pka1/Pkr1 complex is a heterotetramer with 2
611 catalytic subunits and 2 regulatory units. This complex is dissociated in the presence of cAMP
612 [59]. Moreover, the architecture of the functional domains of *Pkr1* include one interaction
613 domain/dimerization at amino acids 2 to 40 and two cAMP binding domains at amino acids
614 219 to 351 and 353 to 473, based on INTERPRO data (Fig 8D). Consequently, the cAMP binding
615 domain on Pkr1 is critical for the dissociation of the PKA1/PKR1 complex. Analysis of

616 differences in titan cell production, combined with complete genome sequencing, allowed us
617 to identify naturally occurring mutations in the *PKR1* gene that impact titan cell production.
618 Both *PKR1* mutations have a stop codon (Gly125fs for AD2-06 and Asp14fs for Bt58) that
619 reduces the protein length. Interestingly, AD2-06a was the incident clinical isolate and a
620 recurrent isolate recovered after 13 days of amphotericin treatment (AD2-07) did not harbor
621 this PKR1 mutation. In addition, a *PKR1* mutation leading to intron retention was found in a
622 relapse isolate [60] and shown to be associated with less virulence than the incident isolate.
623 Whether the virulence differences observed with the relapse isolates are linked to titan cell
624 formation needs to be further investigated.

625 We identified *TSP2* as a negative regulator of titan cell formation based on deletion
626 mutants and complemented strains. *TSP2* is known to interact with the cAMP/PKA pathway -
627 *tsp2Δ* mutant strains phenotype are reversed by the addition of cAMP [57]. These data suggest
628 that *TSP2* inhibits the cAMP pathway and reinforces the major role of cAMP in titan cell
629 formation. No natural *TSP2* mutants were observed in our collection of clinical isolates.

630 Interestingly, all isolates from the VNBII have a mutation in the *CAC1* gene leading to
631 the functional defect of the Cac1 protein. Out of the six VNBII isolates (S3 Table), only Bt88
632 that harbored an additional functional abolition of Usv101 was able to produce as much titan
633 cells as H99O did. Therefore, in Bt88, titan cell formation resulted in the equilibrium between
634 the abolition of CAC1 (positive regulator) and USV101 (negative regulator).

635 Altogether, these results show proof of concept that our *in vitro* protocol can be used
636 to identify and characterize genes required for titan cell production. Our preliminary analysis
637 only identified a handful of genes involved in titan cell production, but it is likely that many
638 more are involved in generation of this complex cell morphology. Our data provide new
639 insights into the genesis of titan cells and the environmental, host and genetic factors that

640 influence their production. Finally, our data show that this *in vitro* protocol can be used to
641 reproducibly generate titan cells that have similar characteristics to titan cells generated *in*
642 *vivo*. The conditions identified for titan cell formation provide a robust system that could be
643 invaluable to dissect the molecular mechanisms that underlie titan cell formation and allow
644 the identification of naturally occurring mutations that regulate titan cell formation. These
645 studies will enhance our understanding of the impact and mechanisms of yeast morphological
646 changes on pathobiology.

647 **Material and methods**

648

649 **Ethics statement**

650 Mice (purchased from Jackson Laboratories, Bar Harbor, ME) were handled in accordance with
651 guidelines defined by the University of Minnesota Animal Care and Use Committee (IACUC),
652 under approved protocol numbers 1010A91133 and 130830852, and in accordance with the
653 protocols approved by JHSPH IACUC protocol M015H134. All animal experiments were
654 performed in concordance with the Animal Welfare Act, United States federal law, and NIH
655 guidelines.

656

657 **Strains and culture medium**

658 The strains and clinical isolates of *C. neoformans* used in the study are listed in S4 Table. The
659 study was started with H99 strain called H99O that was kindly provided by J. Heitman (Duke
660 University, Durham, NC) in the late 90's. The reference strain KN99α and strains from the
661 Madhani collection were provided from Kirsten Nielsen's lab and the Fungal Genetic Stock
662 Center [61], respectively.

663 *C. neoformans* strains were grown in liquid Yeast Peptone Dextrose (YPD, 1% yeast extract (BD
664 Difco, Le Pont de Claix, France) 2% peptone (BD Difco), 2% D-glucose (Sigma, Saint Louis,
665 Minnesota, USA)) and in minimal medium (MM, 15mM D-glucose (Sigma), 10 mM $MgSO_4$
666 (Sigma), 29.4mM KH_2PO_4 (Sigma), 13mM Glycine (Sigma) , 3.0 µM Thiamine (Sigma), [32]).
667 Minimum inhibitory concentration (MIC) of H99O for fluconazole (FLC) and flucytosine (5FC)
668 (both purchased from Isachim, Shimadzu Group Company, Illkirch-Graffenstaden, France)
669 were determined by the EUCAST method and were 8 and 4 mg/L, respectively.

670

671 ***In vitro* protocol for titan cells generation**

672 *C. neoformans* strain from stock cultures stored in 20% glycerol at -80°C was cultured on
673 Sabouraud agar plate at room temperature (step 1). After 2 to 5 d of culture, approximately
674 10^7 cells were suspended in 10 mL YPD in a T25cm^3 flask and cultured 22 h at 30°C, 150 rpm
675 with lateral shaking until stationary phase (final concentration=2x10^8cells/mL) (step 2). Then,
676 one mL of the suspension was washed twice with MM. The cell concentration was adjusted to
677 10^6 cells/mL in MM and the suspension was incubated in a 1.5 mL tube (Eppendorf) with the
678 cap closed, at 30°C, 800 rpm for 5 d using an Eppendorf Thermomixer (Hamburg, Germany)
679 (step 3). Cell size was determined as described below. Cells with body size >10 µm were
680 considered as titan cells as described [12]. Results are expressed as median cell size
681 [interquartile range, IQR] or as median [IQR] of the proportion of titan cells in a given condition
682 for H99 or as a ratio compared to the proportion of titan cells obtained with the H99O in
683 experiments involving other strains (clinical isolates, other H99 strains and mutants). In
684 specific experiments, 10^4 cells/mL were incubated in 100 well plate (Fischer Scientific) and
685 incubated at 30°C with agitation in the Bioscreen apparatus (Fischer Scientific).
686 In specific experiment using P_{GAL7} inducible mutants in H99, MM with galactose at 15mM
687 (galactose MM) was used in parallel to MM containing glucose (see above).
688

689 **Capsule size analysis**

690 Yeasts were observed after India ink staining and capsule thickness was determined as the
691 size of the thickness in pixel of the white area surrounding the cell wall imaged with an
692 Olympus AX 70 microscope and analyzed using the ImageJ software available at
693 https://imagej.nih.gov/ij/ and the Multi_measures plugin.
694

695 **Chitin content and capsule structure quantification**

696 Multispectral flow cytometry was used to quantify chitin content after calcofluor white
697 staining (CFW, fluorescent brightener 28, 0.0001 µg/mL CFW in PBS) and capsule structure
698 after immunostaining of three anti-capsular antibodies (E1 IgG1 monoclonal antibody [50],
699 both 2D10 [29] and 13F1 [29] IgM monoclonal antibody 30 m at 10 µg/mL) and then
700 incubation with FITC coupled anti-IgG or -IgM secondary antibodies (15 m at 1:1000
701 concentration in PBS). The antibody 18B7 has not been used for this specific experiment
702 because it produces aggregation that prevented ImagestreamX testing. Pictures were taken
703 in flow and analyzed using various existing algorithms. We used ImageStreamX with the
704 INSPIRE software (Amnis Corporation). Cell suspensions were adjusted to 10^7 in 200 µL and
705 10,000 cells were recorded at 40-fold magnification in 3 different channels including the bright
706 field channel (BF) and 2 fluorescence channels (channel 1: 430-505nm [CALCO]; channel 2:
707 470-560nm [Anticapsular antibodies]). Data analysis was performed using the IDEAS software
708 (Amnis Corporation) after fluorescence compensation procedures. The first step consists in
709 the definition of a mask that delineates the relevant pixels in each picture. Then, 54 algorithms
710 (calculations made for each event within a defined mask) are available to analyze size, texture,
711 location, shape or signal strength. Using basic algorithms, unfocused events, yeasts aggregates
712 were excluded [4]. First titan cells (TC) and typical cells (tC) were selected based on a dot plot
713 Area/Diameter. We decided to avoid overlap between populations and select well separated
714 population based on their size after control using the bar added on the picture of the yeasts
715 (see Fig 2A-2B). For chitin content, the calcofluor intensity histogram using the Intensity of
716 algorithm in channel 01 have been generated for TC and tC (see Fig 2C-2D). For capsule
717 structure, the algorithms dedicated to structure analysis were tested and Modulation and
718 Bright details intensity R7 algorithms in channel 2 have been found to separate the capsule

719 structure of titan cells from typical cells populations. For each population of interest, the
720 geometric mean was calculated using the IDEAS software.
721 Additional experiments using fluorescence microscopy for chitin content measurement was
722 performed after calcofluor white staining (CFW, fluorescent brightener 28) adapted from [42].
723 Briefly, 10^7 *C. neoformans* cells in 10 mL MM were washed once and 500 µL of 3.7%
724 formaldehyde in PBS was added. Cells were incubated at room temperature for 30-40 m,
725 inverting the tube every 5 m. Samples were washed twice in PBS, cell concentration was
726 adjusted to 10^6 cell/mL. The supernatant was removed and 1 mL of 0.0001 µg/mL CFW in PBS
727 was added, and incubated 5 m at 25°C. Cells were then washed twice in PBS. Results were
728 expressed as median [IQR] of the mean fluorescence intensity/pixel/cell after picture analysis
729 as described below.
730
731 **Capsule immunofluorescence and melanization analysis**
732 Capsule immunofluorescence (IF) of titan cells was done by incubating approximately $5x10^6$
733 cells/mL with 10µg/mL of murine-derived monoclonal antibodies to the cryptococcal capsule
734 (IgG1 18B7, IgG1 E1, IgM 12A1, IgM 2D10 [29,50] in blocking solution (1% bovine serum
735 albumin in PBS). Cells and mAb mixtures were done in 1.5 mL microcentrifuge tubes at 37 °C
736 for 1 h under continuous mixing. Next, cells were washed three times with PBS by
737 centrifugation (5,000 rpm for 5 m at room temperature) and incubated for 1 h at 37 °C with 5
738 µg/mL fluorescently labelled secondary-mAbs, goat anti-mouse IgG1-FITCs or IgM-TRITCs
739 (Southern Biotech) in blocking solution and 1 µg/mL of Uvitex2b (Polysciences, Warrington,
740 PA) solution to visualize the fungal cell wall. Cells were washed three times with PBS by
741 centrifugation, mounted in glass coverslips and imaged with an Olympus AX 70 microscope
742 equipped with blue, green and red fluorescent filters using 40x and/or oil immersion 100x

743 objectives. Capsule immunofluorescence of titan cells preparations performed in two
744 independent experiments gave consistent results.
745 Titan cells melanization was induced following step 3. Cells were washed once with minimal
746 medium, suspended in 1mL of minimal medium supplemented with 1mM of L-DOPA (Sigma
747 D9628), transferred to a 5mL Erlenmeyer flask (for normal oxygenation) and incubated at 30
748 °C under continuous mixing at 200 rpms for 3 d. Since melanin is resistant to acid hydrolysis,
749 a spherical melanin "ghost" remains following incubation of black cells with 12N HCl for 1 h at
750 100 °C (a reduced and modified version of the procedure in [62]. Acid-resistant melanin
751 "ghosts" were washed three times in PBS by centrifugation and visualized using light
752 microscopy.
753 Melanization was measured using imageJ in Icy software by manually circling each cell and
754 measuring the mean gray intensity / pixel /cell. Blackness was calculated as the maximum
755 mean grey intensity minus the mean grey intensity / pixel /cell. Increasing melanin content
756 will result in higher blackness.
757
758 **N-acetylglucosamine quantification**
759 H99 cells were grown in MM for 48 h *in vitro*. Cells were centrifuged 2 m at 14,000 rpm and
760 were then washed twice with sterile water. These cells were exposed to γ-radiation to remove
761 layers of the capsule polysaccharide [13]. Cells resuspended in sterile water were transferred
762 to a 24-well flat-bottom plate and irradiated for 45 m: dose 560 Gy (56,000 rad).
763 titan cells and tyical cells were separated [20]. Washed irradiated cells were filtered using
764 CellMicroSieves (BioDesign Inc. of New York, Carmel, NY) with a 10 µm pore size. The
765 CellMicroSieves were rinsed with PBS to remove typical cells from the filter. To recover the
766 titan cells population, the CellMicroSieves were inverted and the membrane was washed with

767 PBS. The TCs population was concentrated by centrifugation at 12,000 g for 1 m. To recover
768 the typical cells population, the filter flow-through was concentrated by centrifugation at
769 12,000 g for 1 m.
770 Cellular chitin quantification was adapted from [63]. Purified *in vitro* titan cells and typical cells
771 were collected by centrifugation at 14,000 rpm for 2 m and the media were removed. Dry
772 weights were measured following 2-3 d of evaporation at 37°C. Dried pellets were extracted
773 with 1 mL 6% KOH at 80°C for 90 m. Samples were centrifuged at 14,000 rpm for 20 m. Each
774 pellet was suspended in 1 mL PBS and spun again. Each pellet was suspended in 0.2 mL of
775 McIlvaine's Buffer (0.2 M Na2HPO4, 0.1 M citric acid, pH 6.0). Five µL of purified *Streptomyces*
776 *griseus* chitinase (5 mg/mL in PBS) was added to hydrolyze chitin to Glu-cNAc and incubated
777 for 3 d at 37°C. Chitinase-treated samples were spun at 14,000 rpm for 1 m, each 10 µL of
778 sample supernatant was combined with 10 µL 0.27 M sodium borate, pH 9.0. Samples were
779 heated to 99.9°C for 10 m. Upon cooling to room temperature, 100 µl of DMAB solution
780 (Ehrlich's reagent, 10 g p-dimethylaminobenzaldehyde in 12.5 mL concentrated HCl, and 87.5
781 mL glacial acetic acid) was added, followed by 20 m incubation at 37°C. Hundred µL was
782 transferred to 96-well plates, and absorbance at 585 nm was recorded. Standard curves were
783 prepared from stocks of 0.2 to 2.0 mM of Gluc-NAc (Sigma, Saint Louis, Missouri, USA). The
784 amount of Gluc-NAc was calculated as mmol/g cells (dry weight). Results are expressed as
785 median [IQR].
786
787 **DNA content measurement**
788 A 96-well microtiter plate was filled with 200 µL of a 10^6/mL cell suspension in PBS and
789 centrifuged 5 m at 4000 rpm. The pellet was suspended in 150 µL of ethanol 70% and
790 incubated in the dark 1 h at 4°C. After discarding the supernatant, a 50 µL mix composed of

791 44 µL NS (0.01M Tris HCL pH 7.2, 1 mM EDTA, 1mM CaCl2, 0.25 M Sucrose, 2.12 mM $MgCl_2$,
792 0.1 mM $ZnCl_2$), 5µL RNase A at 10mg/mL and 1.25µL PI at 0.5mg/mL was added in each well
793 as described [64]. After a 30 m incubation at 30°C in the dark, the plate was sonicated 1 m and
794 each sample diluted at 1:40 in 50mM Tris HCl. The fluorescence intensity was measured using
795 the Guava easyCyte 12HT Benchtop Flow Cytometer (Guava, MERCK, Kenilworth, New Jersey).
796 Selection of singlets by gating allowed (i) determination of PI intensity on channel YelB
797 (583/26) in FSC/SSC^{high} (TC) and FSC/SSC^{low} (tC); (ii) determination of the FSC/SSC distribution
798 in PI^{high} and PI^{low} population. FlowJo software v.10 was used to analyze the data. The graphs
799 of the number of yeasts were normalized to the mode to depict the data in terms of '% of
800 max'. The % of max denotes the number of cells in each bin (the numerical ranges for the
801 parameter on the *x* axis) divided by the number of cells in the bin that contains the largest
802 number of cells.
803
804 **Determination of the ancestry of titan cells by flow cytometry**
805 Knowing that CFW staining does not alter *C. neoformans* viability and that daughter cells
806 harbored lower CFW signal due to partial cell wall transmission from mother to daughter cells
807 [4,30], we analyzed cell size and CFW fluorescence intensity of the progenies of titan cells and
808 typical cells following the *in vitro* protocol on 10^6 cells of H99O pre-stained with CFW (channel
809 BluV 448/50 using Guava).
810
811 **Dynamic imaging**
812 Budding rates were determined after yeasts (10^5 cells composed of titan cells and typical cells)
813 previously incubated using our protocol or *in vivo* (see below) were directly deposited in a 35
814 mm sterile culture dish in minimal medium without agitation and incubated at 30°C. Pictures

815 were taken every 2 or 5 m by phase microscopy using the Axiovert 200M inverted microscope
816 with 40X or 20X objectives (Carl Zeiss MicroImaging, NY), used in conjunction with an
817 AxiocamMR camera.
818 Cell size evolution over time was assessed for strain AD2-06a by dynamic imaging (Nikon
819 Biostation). Briefly, 35 mm sterile culture dish (Hi-Q4, Nikon) were coated for 1 m with E1
820 antibody at 2 mg/L in order to provide anchor for the capsule. Yeasts (10^5 cells) were added
821 in 1 mL MM and incubated at 32°C for 18 h. Series of 221 images were taken by phase-contrast
822 microscopy every 5 m at ×100 magnification. Merging was done using ImageJ software in Icy
823 Software.
824
825 **Impact of various factors on titan cells generation**
826 To analyze the various factors that could impact titan cells generation, we modified the various
827 steps of our *in vitro* protocol. For step1, stress was produced by 8 subcultures (twice a week
828 for one month) on agar medium or on agar supplemented with CFW (20mg/L) or with
829 fluconazole (32mg/L). For step 2, the pH of MM (normally at 5.5) was set at 4, 7 or 8.5 without
830 buffering. For step 3, initial cell concentration (from 10^4 to 10^7cells/mL) was tested. Hypoxia
831 was generated physically by closing the cap of the Eppendorf tube during 5 d or chemically
832 upon incubation in MM supplemented with 1 nM $CoCl_2$, cap closed, as already described [65].
833 The production of titan cells was also assessed in the presence of various reagents added at
834 step 3: (1) Qsp1 peptide (NFGAPGGAYPW, [33]) (Biomatik, Cambridge, Canada) was
835 resuspended at 10mM in water and stored at -80°C until use at 10 µM final with the scrambled
836 peptide (AYAPWFGNPG) as a control; (2) pantothenic acid purchased from Sigma (Saint-Louis,
837 Missouri, USA) used at 125 µM; (3) monoclonal anti-capsular antibodies E1 [50] and 18B7 [51]
838 used at a final concentration of 166 µg/mL in MM [66]; (4) decomplemented fetal calf serum

839 (FCS, Invitrogen, Carlsbad, CA, USA) at 5 % in MM; (5) L-α-Phosphatidylcholine from egg yolk
840 (Sigma, Saint-Louis, Missouri, USA) was extemporaneously reconstituted at 5 mM in MM; (6)
841 antifungal drugs (fluconazole and flucytosine) were tested at the concentrations close to the
842 MIC (2-fold dilutions) with the diluent (DMSO or water) as control. Results are expressed as
843 median [IQR]. Growth in the presence or in the absence of antifungal drugs was evaluated by
844 enumeration of yeast cells concentration at step 4 of our protocol using the Guava cytometer,
845 starting from 10^6 cells inoculated at step 1.

846

847 **Production and isolation of titan cells from infected mice**

848 *C. neoformans* strains were cultured overnight at 30°C in YPD broth medium (BD, Hercules,
849 Canada). Yeast cells were collected by centrifugation, washed with phosphate buffered saline
850 PBS and resuspended in sterile saline. For titan cells analysis *in vivo*, groups of 6- to 8-week-
851 old C57BL/6J mice (Jackson Labs, Bar Harbor, Maine) were anesthetized by
852 5% isofurane inhalation for 1-5 m, infected intranasally with 2×10^5 cells in a 40 µL volume
853 and sacrificed at D6. In these experiments, 84% of titan cells were obtained. For mutant
854 screening, groups of 6- to 8-week-old C57BL/6J mice (Jackson Labs, Bar Harbor, Maine) were
855 anesthetized by intraperitoneal pentobarbital injection and infected intranasally with $5 \times$
856 10^6 cells in a 50 µL volume. Infected mice were sacrificed by CO_2 inhalation at 3 d post-
857 infection. The lungs were harvested, homogenized, and then resuspended in 10 mL PBS
858 supplemented with collagenase (1 mg/mL) [13]. Cell homogenates were incubated for 1 hour
859 at 37°C with agitation, and washed several times with double distilled water. The *C.*
860 *neoformans* cells were fixed with 3.7 % formaldehyde for 40 m, washed 3 times with sterile
861 PBS, and then resuspended in sterile PBS. The proportion of titan cells and typical cells were

862 determined by microscopy. Data presented were from 3 mice per strain, except for strains
863 *sgf29Δ* in H99O, H99S that had 2 mice per strain.
864
865 **Mutant generation**
866 We PCR amplified the *PKR1* and *TPS2* genes using the primer KN99α DNA as substrate and the
867 following primers (PKR1F: AAGCTTggaatgaagatgaaattagtacgtg; PKR1R:
868 ACTAGTgtccatcattgctgtaacttggttg; TSP2F: GAGCTCaactccgatgatcatggactcgg; TSP2R:
869 GAGCTCtgcccaagagactagagtgtaacc). The 2559 bp TPS2 and the 2000 bp PKR1 amplicons were
870 cloned in the pGEMT easy vector (Clontech) and sequenced. The pNE609 and pNE610
871 plasmids were then constructed by cloning the *PKR1* and *TPS2* DNA fragments into the
872 pSDMA57 plasmid [67] using the SpeI/HindIII and SacI cloning sites, respectively.
873 To create transformants, the plasmids pSDMA57 containing PKR1 amplicon was linearized
874 with BaeI and biolistically transformed into AD2-06a and Bt156 clinical strains. To complement
875 the *tsp2Δ* mutant, pSDMA57 plasmid containing *TSP2* gene was linearized with BaeI and
876 biolistically transformed into the *tsp2Δ* mutant strain. All transformants were selected on YPD
877 supplemented with neomycin. Genomic DNA was purified from the transformants and PCR
878 was used to check the presence of *PKR1* and *TSP2* genes in the transformed strains. PCR
879 reactions contained 1 µl gDNA, 2.5 µl of each of the 10 mM primer stocks (PKR1 forward, PKR1
880 reverse, TSP2 forward, TSP2 reverse) 5 µl Taq buffer, 4 µl dNTPs, 0.25 µl ExTaq polymerase
881 (New England Biolabs, USA) and 34.75 µl sterile water. The cycling parameters were 35 cycles
882 of 94°C for 20 seconds, 54°C for 20 seconds and 72°C for 90 seconds. Products were visualized
883 using electrophoresis with 0.8% TAE agarose gel. To differentiate between random
884 integration, single insertion, and tandem insertion into the safe haven, we performed a similar

885 PCR as above using primers UQ1768, UQ2962, UQ2963, and UQ3348 as previously described
886 [67].
887
888 **DNA Sequencing, variant identification, and bioinformatic analysis**
889 Genomic DNA was adapted for Illumina sequencing using Nextera reagents. Libraries were
890 sequenced on an Illumina HiSeq to generate 101 base reads. most data was previously
891 described [39,68] and one additional isolate was newly sequenced for this study (AD2-07)
892 (NCBI SRA accession SRR5989089). Reads were aligned to the *C. neoformans* H99 assembly
893 (GenBank accession GCA_000149245.2 [34] using BWA-MEM version 0.7.12 [69]. Variants
894 were then identified using GATK version 3.4 [70], where indels were locally realigned,
895 haplotypeCaller was invoked in GVCF mode with ploidy = 1, and genotypeGVCFs was used to
896 predict variants in each strain. All VCFs were then combined and sites were filtered using
897 variantFiltration with QD < 2.0, FS > 60.0, and MQ < 40.0. Individual genotypes were then
898 filtered if the minimum genotype quality < 50, percent alternate allele < 0.8, or depth < 5.
899 Variants were then functionally annotated with SnpEff version 4.2 [71]. For phylogenetic
900 analysis, the 535,968 sites with an unambiguous SNP in at least one isolate and with ambiguity
901 in at most 10% of isolates were concatenated; insertions or deletions at these sites were
902 treated as ambiguous to maintain the alignment. Phylogenetic trees were estimated using
903 RAxML version 8.2.4 [72] under the GTRCAT model in rapid bootstrapping mode. For
904 determination of Pkr1 architecture domains, the INTERPRO tool was used
905 (http://www.ebi.ac.uk/interpro/protein/J9VH50).
906
907 **Pictures analysis using Icy software and statistical analysis**

908 To increase the number of events analyzed in each condition tested/each parameter analyzed
909 (cell size, capsule size and chitin content), pictures of 3-5 fields were taken with an AxioCam
910 MRm camera (Carl Zeiss, Oberkochen) at x40 on interferential contrast microscope (DMLB2
911 microscope; Leica, Oberkochen). Image were then analyzed (for cell size and chitin content)
912 using Icy software v.1.9.2.1.[73] (icy.bioimageanalysis.org) and a specific plugin (HK-Means
913 plugin (http://icy.bioimageanalysis.org/plugin/HK-Means) that allows analysis of multiple
914 structures from a bright field. Preliminary experiments were done to compare results obtained
915 with Icy to "manual" measurements by analyzing about 200 cells on the same pictures for 3
916 independent experiments. In subsequent experiments, results were pooled for a given
917 condition from 2 to 3 independent experiments after good reproducibility was assessed.
918 Statistical analysis was performed with STATA software (College Station, Texas, v13.0). To
919 validate the cell size determination using the Icy software, the intraclass correlation
920 coefficient was calculated. The ability of the automated method to classify the *C. neoformans*
921 cells as titan cells or typical cells compared to visual measurement was evaluated using the
922 Kappa test [74]. To compare titan cells generation in the various conditions, non-parametric
923 tests were performed using the Kruskal-Wallis test for multiple comparisons or Mann Whitney
924 test as required. GraphPad Prism software (v.6) was used to generate graphs.
925
926 **Accession numbers**
927 All sequence data from this study have been submitted to NCBI BioProject
928 (https://www.ncbi.nlm.nih.gov/bioproject) under accession number PRJNA174567.
929 The AD2-07 sequence is available in the NCBI SRA under the accession number SRR5989089
930 (https://www.ncbi.nlm.nih.gov/sra/SRR5989089/)
931

932 **Acknowledgments**

933 We warmly thank Pr James Kronstad and Melissa Caza for sending us their collection of
934 deletion and complemented mutants of the *PKR1* gene, as well as their PGal:PKR1 and
935 PGal:PKA conditional mutants. We thank Dr Tihana Bicanic, Shichina Kannmbath, Charles
936 Giamberardino and Jennifer Tenor who kindly provided specific clinical isolates. The authors
937 want to thank Marie Desnos-Ollivier for her help with Sanger sequencing, JL Tinevez for
938 technical assistance in Biostation experiments, Stéphane Dallongeville for help with Icy
939 Software, Stevenn Volant for biostatistics, Pierre-Henri Commere for FACS analysis,
940 Frederique Moyrand for performing PCR and plasmid preparations. We thank Quigly
941 Dragotakes for helping us determining cell and capsule sizes in specific experiments. The
942 authors acknowledge Hiten Madhani and members of his laboratory for the gene deletion
943 collection that has been made available ahead of publication to the scientific community.

944

945

946 **References**

947 1. Rajasingham R, Smith RM, Park BJ, Jarvis JN, Govender NP, Chiller TM, et al. Global burden of
948 disease of HIV-associated cryptococcal meningitis: an updated analysis. Lancet Infect Dis. 2017;17:
949 873. doi:10.1016/s1473-3099(17)30243-8
950 2. Park BJ, Wannemuehler KA, Marston BJ, Govender N, Pappas PG, Chiller TM. Estimation of the
951 current global burden of cryptococcal meningitis among persons living with HIV/AIDS. AIDS Lond
952 Engl. 2009;23: 525–530. doi:10.1097/QAD.0b013e328322ffac
953 3. Garcia-Hermoso D, Janbon G, Dromer F. Epidemiological evidence for dormant *Cryptococcus*
954 *neoformans* infection. Cryptococcus Neoformans. 1999;37: 3204–3209.
955 doi:10.1128/9781555818241.ch15
956 4. Alanio A, Vernel-Pauillac F, Sturny-Leclère A, Dromer F. *Cryptococcus neoformans* host adaptation:
957 toward biological evidence of dormancy. mBio. 2015;6: e02580-14. doi:10.1128/mBio.02580-14
958 5. Chrétien F, Lortholary O, Kansau I, Neuville S, Gray F, Dromer F. Pathogenesis of cerebral
959 *Cryptococcus neoformans* infection after fungemia. J Infect Dis. 2002;186: 522–530.
960 doi:10.1086/341564
961 6. Choi J, Vogl AW, Kronstad JW. Regulated expression of cyclic AMP-dependent protein kinase A
962 reveals an influence on cell size and the secretion of virulence factors in *Cryptococcus neoformans*.
963 Mol Microbiol. 2012;85: 700. doi:10.1111/j.1365-2958.2012.08134.x
964 7. Franzot SP, Mukherjee J, Cherniak R, Chen LC, Hamdan JS, Casadevall A. Microevolution of a
965 standard strain of *Cryptococcus neoformans* resulting in differences in virulence and other
966 phenotypes. Infect Immun. 1998;66: 89–97.
967 8. Hu G, Cheng P-Y, Sham A, Perfect JR, Kronstad JW. Metabolic adaptation in *Cryptococcus*
968 *neoformans* during early murine pulmonary infection. Mol Microbiol. 2008;69: 1456–1475.
969 doi:10.1111/j.1365-2958.2008.06374.x
970 9. Gerstein AC, Nielsen K. It's not all about us: evolution and maintenance of *Cryptococcus* virulence
971 requires selection outside the human host. Yeast. 2017;34: 143. doi:10.1002/yea.3222
972 10. Brown SM, Campbell LT, Lodge JK. *Cryptococcus neoformans*, a fungus under stress. Curr Opin
973 Microbiol. 2007;10: 320–325. doi:10.1016/j.mib.2007.05.014
974 11. Wang L, Lin X. Morphogenesis in Fungal Pathogenicity: Shape, Size, and Surface. PLOS Pathog.
975 2012;8: e1003027. doi:10.1371/journal.ppat.1003027
976 12. Okagaki LH, Strain AK, Nielsen JN, Charlier C. Cryptococcal cell morphology affects host cell
977 interactions and pathogenicity. PLoS Pathog. 2010;6: e1000953.
978 doi:10.1371/journal.ppat.1000953
979 13. Zaragoza O, García-Rodas R, Nosanchuk JD, Cuenca-Estrella M, Rodríguez-Tudela JL, Casadevall A.
980 Fungal cell gigantism during mammalian infection. PLoS Pathog. 2010;6: e1000945.
981 doi:10.1371/journal.ppat.1000945
982 14. Love GL, Boyd GD, Greer DL. Large *Cryptococcus neoformans* isolated from brain abscess. J Clin
983 Microbiol. 1985;22: 1068–1070.
984 15. Cruickshank JG, Cavill R, Jelbert M. *Cryptococcus neoformans* of unusual morphology. Appl
985 Microbiol. 1973;25: 309–312.
986 16. García-Rodas R, Casadevall A, Rodríguez-Tudela JL, Cuenca-Estrella M, Zaragoza O. *Cryptococcus*
987 *neoformans* capsular enlargement and cellular gigantism during *Galleria mellonella* infection. PloS
988 One. 2011;6: e24485. doi:10.1371/journal.pone.0024485
989 17. Zaragoza O, Nielsen K. Titan cells in Cryptococcus neoformans: cells with a giant impact. Curr Opin
990 Microbiol. 2013;16: 409–413. doi:10.1016/j.mib.2013.03.006
991 18. Okagaki LH, Wang Y, Ballou ER, O'Meara TR, Bahn Y-S, Alspaugh JA, et al. Cryptococcal titan cell
992 formation is regulated by G-protein signaling in response to multiple stimuli. Eukaryot Cell.
993 2011;10: 1306–1316. doi:10.1128/EC.05179-11

994 19. Crabtree JN, Okagaki LH, Wiesner DL, Strain AK, Nielsen JN, Nielsen K. Titan cell production
995 enhances the virulence of *Cryptococcus neoformans*. Infect Immun. 2012;80: 3776–3785.
996 doi:10.1128/IAI.00507-12
997 20. Gerstein AC, Fu MS, Mukaremera L, Li Z, Ormerod KL, Fraser JA, et al. Polyploid titan cells produce
998 haploid and aneuploid progeny to promote stress adaptation. mBio. 2015;6: e01340-15.
999 doi:10.1128/mBio.01340-15
1000 21. Okagaki LH, Nielsen K. Titan cells confer protection from phagocytosis in *Cryptococcus neoformans*
1001 infections. Eukaryot Cell. 2012;11: 820–826. doi:10.1128/EC.00121-12
1002 22. Mukaremera L, Nielsen K. Adaptive Immunity to *Cryptococcus neoformans* Infections. J Fungi Basel
1003 Switz. 2017;3. doi:10.3390/jof3040064
1004 23. D'Souza CA, Yue C, Alspaugh JA. Cyclic AMP-dependent protein kinase controls virulence of the
1005 fungal pathogen *Cryptococcus neoformans*. Mol Cell Biol. 2001;21: 3179.
1006 doi:10.1128/mcb.21.9.3179-3191.2001
1007 24. Nichols CB, Perfect ZH, Alspaugh JA. A Ras1-Cdc24 signal transduction pathway mediates
1008 thermotolerance in the fungal pathogen *Cryptococcus neoformans*. Mol Microbiol. 2007;63: 1118–
1009 1130. doi:10.1111/j.1365-2958.2006.05566.x
1010 25. Bahn Y-S, Jung K-W. Stress signaling pathways for the pathogenicity of *Cryptococcus*. Eukaryot Cell.
1011 2013;12: 1564–1577. doi:10.1128/EC.00218-13
1012 26. Hu G, Steen BR, Lian T, Sham AP, Tam N, Tangen KL, et al. Transcriptional Regulation by Protein
1013 Kinase A in *Cryptococcus neoformans*. PLOS Pathog. 2007;3: e42.
1014 doi:10.1371/journal.ppat.0030042
1015 27. Geddes JMH, Caza M, Croll D, Stoynov N, Foster LJ, Kronstad JW. Analysis of the Protein Kinase A-
1016 Regulated Proteome of *Cryptococcus neoformans* Identifies a Role for the Ubiquitin-Proteasome
1017 Pathway in Capsule Formation. mBio. 2016;7: e01862-15. doi:10.1128/mBio.01862-15
1018 28. Casadevall A, DeShaw M, Fan M, Dromer F, Kozel TR, Pirofski L a. Molecular and idiotypic analysis
1019 of antibodies to *Cryptococcus neoformans* glucuronoxylomannan. Infect Immun. 1994;62: 3864–
1020 3872.
1021 29. Cordero RJB, Pontes B, Guimarães AJ, Martinez LR, Rivera J, Fries BC, et al. Chronological aging is
1022 associated with biophysical and chemical changes in the capsule of *Cryptococcus neoformans*.
1023 Infect Immun. 2011;79: 4990–5000. doi:10.1128/IAI.05789-11
1024 30. Alanio A, Desnos-Ollivier M, Dromer F. Dynamics of *Cryptococcus neoformans*-macrophage
1025 interactions reveal that fungal background influences outcome during cryptococcal
1026 meningoencephalitis in humans. mBio. 2011;2: e00158-11. doi:10.1128/mBio.00158-11
1027 31. Chrisman CJ, Albuquerque P, Guimarães AJ, Nieves E, Casadevall A. Phospholipids trigger
1028 *Cryptococcus neoformans* capsular enlargement during interactions with amoebae and
1029 macrophages. PLoS Pathog. 2011;7: e1002047. doi:10.1371/journal.ppat.1002047
1030 32. Albuquerque P, Nicola AM, Nieves E, Paes HC, Williamson PR, Silva-Pereira I, et al. Quorum
1031 sensing-mediated, cell density-dependent regulation of growth and virulence in *Cryptococcus*
1032 *neoformans*. mBio. 2013;5: e00986-13. doi:10.1128/mBio.00986-13
1033 33. Homer CM, Summers DK, Goranov AI, Clarke SC, Wiesner DL, Diedrich JK, et al. Intracellular Action
1034 of a Secreted Peptide Required for Fungal Virulence. Cell Host Microbe. 2016;19: 849–864.
1035 doi:10.1016/j.chom.2016.05.001
1036 34. Janbon G, Ormerod KL, Paulet D, Byrnes EJ, Yadav V, Chatterjee G, et al. Analysis of the genome
1037 and transcriptome of *Cryptococcus neoformans* var. *grubii* reveals complex RNA expression and
1038 microevolution leading to virulence attenuation. PLoS Genet. 2014;10: e1004261.
1039 doi:10.1371/journal.pgen.1004261
1040 35. Arras SDM, Ormerod KL, Erpf PE, Espinosa MI, Carpenter AC, Blundell RD, et al. Convergent
1041 microevolution of *Cryptococcus neoformans* hypervirulence in the laboratory and the clinic. Sci
1042 Rep. 2017;7: 17918. doi:10.1038/s41598-017-18106-2
1043 36. O'Meara TR, Alspaugh JA. The *Cryptococcus neoformans* capsule: a sword and a shield. Clin
1044 Microbiol Rev. 2012;25: 387–408. doi:10.1128/CMR.00001-12

1045 37. Cordero RJB, Casadevall A. Functions of fungal melanin beyond virulence. Fungal Biol Rev. 2017;31:
1046 99. doi:10.1016/j.fbr.2016.12.003
1047 38. Rhodes J, Desjardins CA, Sykes SM, Beale MA, Vanhove M, Sakthikumar S, et al. Tracing Genetic
1048 Exchange and Biogeography of *Cryptococcus neoformans* var. *grubii* at the Global Population
1049 Level. Genetics. 2017; doi:10.1534/genetics.117.203836
1050 39. Desjardins CA, Giamberardino C, Sykes SM, Yu C-H, Tenor JL, Chen Y, et al. Population genomics
1051 and the evolution of virulence in the fungal pathogen *Cryptococcus neoformans*. Genome Res.
1052 2017;27: 1207–1219. doi:10.1101/gr.218727.116
1053 40. Dambuza IM, Drake T, Chapuis A, Taylor-Smith L, LeGrave N, Rasmussen T, et al. The *Cryptococcus*
1054 *neoformans* Titan cell is an inducible and regulated morphotype underlying pathogenesis. bioRxiv.
1055 2017; 190587. doi:10.1101/190587
1056 41. Trevijano-Contador N, Rossi SA, Oliveira HC de, Llorente I, Correia I, Pla J, et al. *Cryptococcus*
1057 *neoformans* can form titan-like cells in vitro in response to multiple signals that require the
1058 activation of several transduction pathways. bioRxiv. 2017; 193540. doi:10.1101/193540
1059 42. Wiesner DL, Specht CA, Lee CK, Smith KD, Mukaremera L, Lee ST, et al. Chitin recognition via
1060 chitotriosidase promotes pathologic type-2 helper T cell responses to cryptococcal infection. PLoS
1061 Pathog. 2015;11: e1004701. doi:10.1371/journal.ppat.1004701
1062 43. Veses V, Richards A, Gow NAR. Vacuoles and fungal biology. Curr Opin Microbiol. 2008;11: 503–
1063 510. doi:10.1016/j.mib.2008.09.017
1064 44. Zhang N, Cao L. Starvation signals in yeast are integrated to coordinate metabolic reprogramming
1065 and stress response to ensure longevity. Curr Genet. 2017; doi:10.1007/s00294-017-0697-4
1066 45. Nizet V, Johnson RS. Interdependence of hypoxic and innate immune responses. Nat Rev Immunol.
1067 2009;9: 609–617. doi:10.1038/nri2607
1068 46. Grahl N, Shepardson KM, Chung D, Cramer RA. Hypoxia and fungal pathogenesis: to air or not to
1069 air? Eukaryot Cell. 2012;11: 560–570. doi:10.1128/EC.00031-12
1070 47. Grahl N, Puttikamonkul S, Macdonald JM, Gamcsik MP, Ngo LY, Hohl TM, et al. In vivo hypoxia and
1071 a fungal alcohol dehydrogenase influence the pathogenesis of invasive pulmonary aspergillosis.
1072 PLoS Pathog. 2011;7: e1002145. doi:10.1371/journal.ppat.1002145
1073 48. Chun CD, Liu OW, Madhani HD. A link between virulence and homeostatic responses to hypoxia
1074 during infection by the human fungal pathogen *Cryptococcus neoformans*. PLoS Pathog. 2007;3:
1075 e22. doi:10.1371/journal.ppat.0030022
1076 49. Lee H, Chang YC, Nardone G, Kwon-Chung KJ. TUP1 disruption in *Cryptococcus neoformans*
1077 uncovers a peptide-mediated density-dependent growth phenomenon that mimics quorum
1078 sensing. Mol Microbiol. 2007;64: 591. doi:10.1111/j.1365-2958.2007.05666.x
1079 50. Dromer F, Salamero J, Contrepois A, Carbon C, Yeni P. Production, characterization, and antibody
1080 specificity of a mouse monoclonal antibody reactive with Cryptococcus neoformans capsular
1081 polysaccharide. Infect Immun. 1987;55: 742–748.
1082 51. Zebedee SL, Koduri RK, Mukherjee J, Mukherjee S, Lee S, Sauer DF, et al. Mouse-human
1083 immunoglobulin G1 chimeric antibodies with activities against *Cryptococcus neoformans*.
1084 Antimicrob Agents Chemother. 1994;38: 1507. doi:10.1128/aac.38.7.1507
1085 52. McClelland EE, Nicola AM, Prados-Rosales R, Casadevall A. Ab binding alters gene expression in
1086 *Cryptococcus neoformans* and directly modulates fungal metabolism. J Clin Invest. 2010;120:
1087 1355–1361. doi:10.1172/JCI38322
1088 53. Geunes-Boyer S, Beers MF, Perfect JR, Heitman J, Wright JR. Surfactant protein D facilitates
1089 Cryptococcus neoformans infection. Infect Immun. 2012;80: 2444–2453. doi:10.1128/IAI.05613-
1090 11
1091 54. Sanglard D, Ischer F, Calabrese D, de Micheli M, Bille J. Multiple resistance mechanisms to azole
1092 antifungals in yeast clinical isolates. Drug Resist Updat. 1998;1: 255. doi:10.1016/s1368-
1093 7646(98)80006-x
1094 55. Loyse A, Dromer F, Day J, Lortholary O, Harrison TS. Flucytosine and cryptococcosis: time to
1095 urgently address the worldwide accessibility of a 50-year-old antifungal. J Antimicrob Chemother.
1096 2013;68: 2435–2444. doi:10.1093/jac/dkt221

1097 56. Bian C, Xu C, Ruan J, Lee KK, Burke TL, Tempel W, et al. Sgf29 binds histone H3K4me2/3 and is
1098 required for SAGA complex recruitment and histone H3 acetylation. EMBO J. 2011;30: 2829–2842.
1099 doi:10.1038/emboj.2011.193
1100 57. Li Z, Bi J, Yang J, Pan J, Sun Z, Zhu X. Requirement of a Tsp2-type tetraspanin for laccase repression
1101 and stress resistance in the basidiomycete *Cryptococcus neoformans*. Appl Environ Microbiol.
1102 2011;78: 21–27. doi:10.1128/AEM.06072-11
1103 58. Gish SR, Maier EJ, Haynes BC, Santiago-Tirado FH, Srikanta DL, Ma CZ, et al. Computational Analysis
1104 Reveals a Key Regulator of Cryptococcal Virulence and Determinant of Host Response. mBio.
1105 2016;7: e00313-16. doi:10.1128/mBio.00313-16
1106 59. Vandamme J, Castermans D, Thevelein JM. Molecular mechanisms of feedback inhibition of
1107 protein kinase A on intracellular cAMP accumulation. Cell Signal. 2012;24: 1610–1618.
1108 doi:10.1016/j.cellsig.2012.04.001
1109 60. Chen Y, Farrer RA, Giamberardino C, Sakthikumar S, Jones A, Yang T, et al. Microevolution of Serial
1110 Clinical Isolates of *Cryptococcus neoformans* var. *grubii* and *C. gattii*. mBio. 2017;8: e00166-17.
1111 doi:10.1128/mBio.00166-17
1112 61. McCluskey K, Wiest A, Plamann M. The Fungal Genetics Stock Center: a repository for 50 years of
1113 fungal genetics research. J Biosci. 2010;35: 119–126.
1114 62. Wang Y, Aisen P, Casadevall A. Melanin, melanin "ghosts," and melanin composition in
1115 *Cryptococcus neoformans*. Infect Immun. 1996;64: 2420–2424.
1116 63. Banks IR, Specht CA, Donlin MJ, Gerik KJ, Levitz SM, Lodge JK. A chitin synthase and its regulator
1117 protein are critical for chitosan production and growth of the fungal pathogen *Cryptococcus*
1118 *neoformans*. Eukaryot Cell. 2005;4: 1902–1912. doi:10.1128/EC.4.11.1902-1912.2005
1119 64. Tanaka R, Taguchi H, Takeo K, Miyaji M, Nishimura K. Determination of ploidy in *Cryptococcus*
1120 *neoformans* by flow cytometry. J Med Vet Mycol Bi-Mon Publ Int Soc Hum Anim Mycol. 1996;34:
1121 299–301.
1122 65. Ingavale SS, Chang YC, Lee H, McClelland CM, Leong ML, Kwon-Chung KJ. Importance of
1123 mitochondria in survival of *Cryptococcus neoformans* under low oxygen conditions and tolerance
1124 to cobalt chloride. PLoS Pathog. 2008;4: e1000155. doi:10.1371/journal.ppat.1000155
1125 66. McClelland EE, Ramagopal UA, Rivera J, Cox J, Nakouzi A, Prabu MM, et al. A Small Protein
1126 Associated with Fungal Energy Metabolism Affects the Virulence of *Cryptococcus neoformans* in
1127 Mammals. PLoS Pathog. 2016;12: e1005849. doi:10.1371/journal.ppat.1005849
1128 67. Arras SDM, Chitty JL, Blake KL, Schulz BL, Fraser JA. A genomic safe haven for mutant
1129 complementation in *Cryptococcus neoformans*. PloS One. 2015;10: e0122916.
1130 doi:10.1371/journal.pone.0122916
1131 68. Rhodes J, Beale M, Vanhove M, Jarvis JN, Kannambath S, Simpson JA, et al. A population genomics
1132 approach to assessing the genetic basis of within-host microevolution underlying recurrent
1133 cryptococcal meningitis infection. G3 Genes. 2016; doi:10.1101/083469
1134 69. Li H. Aligning sequence reads, clone sequences and assembly contigs with BWA-MEM. 1303;
1135 70. McKenna A, Hanna M, Banks E, Sivachenko A, Cibulskis K, Kernytsky A, et al. The Genome Analysis
1136 Toolkit: a MapReduce framework for analyzing next-generation DNA sequencing data. Genome
1137 Res. 2010;20: 1297–1303. doi:10.1101/gr.107524.110
1138 71. Cingolani P, Platts A, Lily Wang, Coon M, Nguyen T, Wang L, et al. A program for annotating and
1139 predicting the effects of single nucleotide polymorphisms, SnpEff: SNPs in the genome of
1140 *Drosophila melanogaster* strain w1118; iso-2; iso-3. Fly (Austin). 2012;6: 80–92.
1141 doi:10.4161/fly.19695
1142 72. Stamatakis A. RAxML version 8: a tool for phylogenetic analysis and post-analysis of large
1143 phylogenies. Bioinforma Oxf Engl. 2014;30: 1312–1313. doi:10.1093/bioinformatics/btu033
1144 73. de Chaumont F, Dallongeville S, Chenouard N, Hervé N, Pop S, Provoost T, et al. Icy: an open
1145 bioimage informatics platform for extended reproducible research. Nat Methods. 2012;9: 690–
1146 696. doi:10.1038/nmeth.2075
1147 74. The Kappa Statistic in Reliability Studies: Use, Interpretation, and Sample Size Requirements. Phys
1148 Ther. 2005; doi:10.1093/ptj/85.3.257

1149 **Supporting informations**

1150

1151 **S1 Fig. *In vitro* protocol of titan cells generation.** The protocol followed four steps: (1) *C.*
1152 *neoformans* H99O from a frozen stock culture at -80°C was cultured on Sabouraud agar for 2-
1153 5 d; (2) Approximately 10^7 yeasts were then suspended in 10mL of liquid Yeast Peptone
1154 dextrose (YPD) and incubated under agitation (150 rpm) at 30°C for 22 h (stationary phase);
1155 (3) 1 mL of the culture was then washed twice in minimal medium (MM), then 10^6 yeasts were
1156 resuspended in 1mL of minimal medium (MM) Ph5.5, in a 1.5 mL Eppendorf tube and
1157 incubated at 800 rpm for up to 120 h using an Eppendorf thermomixer; (4) A mixture of typical
1158 cells and of titan cells was ready for analysis.

1159

1160 **S2 Fig. Among yeasts recovered at the end of the *in vitro* protocol, those with the highest**
1161 **DNA content have the biggest cell size.**
1162 DNA content was analyzed after propidium iodide (PI) staining of yeast cells obtained at the
1163 end of our protocol (H99O induced), in a control haploid strain (H99O cultured in Sabouraud
1164 agar, H99O-sab) and in a control diploid strain (AD7-77 cultured in Sabouraud agar). Part of
1165 the population of H99O-induced had a higher PI (blue arrow) fluorescence intensity than the
1166 haploid control (upper panel). Gating on the PI intensity showed that the increase in the PI
1167 fluorescence intensity from <20K to >40K corresponded to increase in cell size (FSC) (red
1168 arrows) compared to the diploid (AD7-77) and haploid (H99O Sab) control (lower panel).

1169

1170 **S3 Fig. The FSC^{high}/CFW^{high} population of yeasts correspond to titan cells (TC).**
1171 Cells obtained using our *in vitro* protocol were stained with CFW and sorted by flux cytometry
1172 according to size (FSC) and CFW fluorescence intensity (left panel). Sorted yeasts were

1173 observed using bright field and fluorescence microscopy (right panel) (bar=10µm). Typical
1174 cells (tC) were FSC^{low}/CFW^{low}.
1175
1176 **S4 Fig. Chitin characterization and melanization of titan cells.**
1177 (**A**) Chitin was denser in titan cells (TC) than in typical cells (tC) according to CFW fluorescence
1178 intensity/pixel/cell measured by Icy software after CFW staining (0.01 µg/mL) at step 4 of the
1179 protocol (*p<0.0001). Dots represent individual cells, and boxes median and IQR for 400 cells
1180 each (*p<0.001, pooled measurements from 3 independent experiments). (**B**) N-
1181 acetylglucosamine (GlcNAc), the monomer component of chitin, was increased in titan cells
1182 (TC) compared to typical cells (tC) *in vitro* (left panel) and *in vivo* (right panel) as measured by
1183 a biochemical method after gamma-irradiation of the yeasts to remove the capsule, allowing
1184 a better separation of titan cells and typical cells. Each dot represents result from independent
1185 experiments (n=7). Results are presented as median and IQR (p<0.001). (**C**) Comparing the
1186 blackness of the cell body of titan cells (TC) and typical cells (tC) upon melanization conditions
1187 showed that titan cells contained more melanin than typical cells. (Bar=10µm). (**D**)
1188 Melanization was more important in titan cells (TC) than typical cells (tC) (*p<0.0001) based
1189 on the calculation of the max - mean grey value/pixel of each melanin ghost measured (n=19
1190 for titan cells and n=531 for typical cells) using the ImageJ in Icy software. Each dot represents
1191 an individual cells and boxes median and IQR.
1192
1193 **S5 Fig. Capsule structure of titan cells.**
1194 (**A**) Using multispectral flow cytometry and capsule staining using anticapsular monoclonal
1195 antibodies (mAb), we discriminated the distribution of titan cells and typical cells with almost
1196 no overlap between both population with 2D10 mAb *in vitro* and *in vivo*, based on the

1197 algorithm modulation and Bright details intensity R7. Overlap in the staining characteristics of
1198 titan cells and typical cells were observed for E1 (IgG1) and 13F1 (IgM) antibodies. (**B**)
1199 Immunofluorescence staining with the anti-capsular mAbs 2D10, 12A1, 18B7, and E1 does not
1200 uncover major differences in capsular structures between titan cells (white arrows) and typical
1201 cells (black arrows). Each panel correspond to the same cells observed after staining with (a)
1202 India ink; (b) calcofluor white; (c) one of the Mabs; (d) merge from c and d. (bar=10µm).
1203
1204 **S6 Fig. Growth is maintained in the presence of antifungals after our protocol.** 10^6 cell/mL
1205 were inoculated at step 1 of our protocol, then cell growth was evaluated by enumerating cell
1206 concentration obtained at step 4 of our protocol using Guava flow cytometer for cell counting.
1207 (**A**) Compared to control, fluconazole did not modify cell growth in MM whereas (**B**)
1208 flucytosine (5FC) reduced it, when used at concentration near the minimum inhibitory
1209 concentration (MIC) for 5 d (*p<0.0001 compared to unexposed control). The fluconazole and
1210 flucytosine MICs for H99O were 8 mg/L and 4 mg/L, respectively. Experiments were done in
1211 triplicates (bars represent mean ± SD). (**C**) Cycloheximide also reduced cell growth at 0.0001
1212 and inhibit cell growth at 0.001 mg/mL (*p<0.0001 compared to unexposed control)
1213
1214 **S7 Fig. Test of iterative subcultures affect titan cells formation with or without the presence**
1215 **of active molecules (CFW or fluconazole)**
1216 Step 1 was modified by sub-culturing H99O 8 times over one month on Sabouraud agar alone
1217 (Sub8), or supplemented with 20mg/L CFW (Sub8+CFW) or with 32mg/L fluconazole
1218 (Sub8+FLC). Compared to initial culture (0Sub), 8 sub-cultures (8Sub) decreased significantly
1219 the cell size (** p<0.0001, vs 0Sub control). In addition, iterative subcultures on CFW and FLC
1220 decreased and increased significantly the cell size compared to the 8Sub control, respectively.

1221 Median and IQR are shown in black for each condition (* p<0.0001 vs 8Sub control). The
1222 numbers above each condition represent the proportion of titan cells observed. The
1223 experiments were performed in triplicate and pooled (mean cell counted ± SD = 2455±913).
1224
1225 **S8 Fig**. **Titan cells generation is dependent on various genes *in vivo*.** (**A**) Strains from the H99
1226 lineage harbored variable abilities to generate titan cells with H99O and KN99α *in vivo*
1227 compared to the other H99 strains (S, L, W, CMO18). (**B**) The *sgf29*Δ and *lmp1*Δ mutant strains
1228 show a decrease in titan cells generation in various H99 backgrounds *in vivo* compared to
1229 H99O and rescued by complementation. Each experiment was done in triplicates. Results are
1230 presented as stacked bar of the proportion of titan cells (titan cells) and regulars cells (typical
1231 cells), * p<0.0001 vs control H99O.
1232
1233 **S9 Fig. The proportion of titan cells generated is dependent on various genes and requires**
1234 **signaling through the Gpr/PKA/Rim101 pathway.**
1235 The different H99 strains harbored variable abilities to produce titan cells compared to H99O
1236 *in vitro* (**A**) and in vivo (**B**). *Sgf29Δ* and *lmp1Δ* deletion mutants show a decrease in titan cells
1237 generation in various H99 backgrounds compared to H99O *in vitro* **(C)** and in vivo **(D)**.
1238 Complementation in strains *lmp1Δ:LMP1* and *sgf29Δ:SGF29* in H99S background restored the
1239 phenotype of H99S. **(E)** Rim101 and *GPR4* and *GPR5* and *CAC1* are required for titan cells
1240 generation *in vitro* in H99 and KN99α. The ratio to the value obtained for H99O used as a
1241 calibrator in each experiment was calculated for each strain. Bar represent mean ± SD (mean
1242 cell counted=600). Khi2 test was performed to compare the experimental conditions to H99O,
1243 they were performed in triplicates and pooled (*p<0.0001, **p<0.0001, when the comparison
1244 was done with the parental strain H99S.)

1245

1246 **S10 Fig. *USV101* and *SRE1* deletion influenced titan cells formation**

1247 (**A**) *usv101Δ* is a repressor of titan cells formation. (**B**) The *sre1Δ* mutant strain decreased
1248 titan cells formation compared to the parental strain KN99α. The ratio to KN99α, used as a
1249 calibrator in each experiment, was calculated for each strain and results expressed as mean
1250 ±SD. To compare the experimental conditions to KN99α, Khi2 analysis was performed
1251 (*p<0.0001).

1252

1253 **S11 Fig. Chr9 ploidy does not influence titan cells generation.** A panel of 7 clinical isolates
1254 with partial Chromosome 9 duplication (left panel) was tested for its ability to generate titan
1255 cells. Only H99O and AD2-06a exhibited increased cell sizes (middle panel). The proportion
1256 of titan cells was 67.9 % (431/667) for AD2-06a, 32.1% (429/1339) for H99O, and 4.2%
1257 (51/1227), for Ug2459 (Khi2 compared to H99O, *p<0.0001) with the ratio of the proportion
1258 of titan cells to that produced in H99O shown in the right panel.

1259

1260 **S12 Fig. *PKR1* mutations influence median cell size**

1261 Strains with *Pkr1* loss of function mutation showed a variable ability to produce titan cells
1262 depending on the resulting truncated proteins. The clinical isolate AD2-07 which did not
1263 harbor the *PKR1* mutation was recovered from the CSF of an HIV-positive patient on d 13 of
1264 amphotericin B treatment while AD2-06a was recovered from its initial CSF. The median cell
1265 size (5.9 µm [5.2-6.6]) was significantly decreased in AD2-07 and increased in AD2-06a (8.5 µm
1266 [7.0-13.0]) compared to H99O (7.7 µm [6.6-9.2]) (p<0.0001). Except Bt156 (median of 7.7 µm
1267 [6.4-9.4]), the others strains had a significantly decreased median size compared to H99O

1268 (p<0.0001), 6.9 µm [6.0-7.8] for 8-1 strain; 6.5 µm [5.8-7.1] for Bt77, 6.4 µm [5.7-7.2] for
1269 Bt117; and 5.4 µm [4.7-6.1] for Ug2462. Experiments were done in triplicate and pooled.
1270
1271 **S13 Fig. Non-synonymous mutation in *USV101* enhances titan cells generation based on**
1272 **clinical isolates analysis.**
1273 Bt88 harbored a truncated Usv101 protein due to a frameshift mutation. The titan cells
1274 generation is negative in Bt31, Bt40, Bt89, Bt105 and Bt133 and increased for Bt88 with a ratio
1275 at 0.6±0.4 and a proportion of titan cells of 21.6% (423/1958) compared to H99O 38.5%
1276 (729/1890). Experiments were done in triplicate and pooled.
1277
1278 **S1 Movie. Time lapse imaging of titan cells and typical cells generated *in vitro* (after 5 d)**
1279 **allowed to grow.** Titan cells produced normal sized daughter cells upon incubation in fresh
1280 MM (at 30°C, one picture every 2min during 24 h).
1281
1282 **S2 Movie. Time lapse imaging of titan cells and typical cells generated *in vivo* (6 d post**
1283 **infection, intranasal route) allowed to grow.** Titan cells produced normal sized daughter cells
1284 upon incubation in fresh MM (at 30°C, one picture every 5 m during 24 h at ×400 magnification
1285 using transmitted light (white bar=10 µm, NC = typical cells)**.**
1286
1287 **S3 Movie. Time lapse imaging showing mothers cells increasing in time allowing titan cells**
1288 **generation first produced between 8 and 12 h of incubation.**
1289 Dynamic imaging of yeasts from the AD2-06a *C. neoformans* clinical isolate using the Nikon
1290 Biostation IM. Yeasts were seeded in MM on a culture dish that was previously coated with

1291 E1 at 2 mg/L. Images were taken every 5 m for 24 h at ×100 magnification using transmitted

1292 light (white bar=10 μm)

1293

1294 **S1 Table.** Gene disrupted in AD2-06a but not in closely related isolated AD3-55a or AD3-41a

1295

1296 **S2 Table.** Clinical isolates with chromosome 9 ploidy variation

1297

1298 **S3 Table.** Strains harboring Pkr1 loss-of-function mutations used in this study

1299

1300 **S4 Table.** Strains used in this study

1301

1302 **Figures and Tables**

1303

1304 **Fig 1. Titan cells generated *in vitro* harbor the typical phenotype of titan cells produced *in***

1305 ***vivo*.**

1306 (**A**) Specific morphology of titan cells (TC, white arrow) *in vitro* (left panel) and *in vivo* (right

1307 panel) was observed: enlarged capsule (a), increased cell body size > 10 µm (b), thickened cell

1308 wall, large central vacuole, and peripheral cell cytoplasm distribution) while the size of typical

1309 cells (tC, white arrow) is <10 µm. (**B**) Titan cells were reproducibly generated in lab 1 using

1310 H99O and in two independent laboratories (lab 2 and lab 3) using their local H99O strain. Cell

1311 size was measured manually or by using the Icy software on pictures taken in bright field. Each

1312 dot represents an independent experiment (median [interquartile range, IQR] are presented);

1313 (**C**) Cell body size is increased *in vivo* compared to *in vitro*. Dots represent individual cells, and

1314 boxes median and IQR for 230 cells each (*p<0.0001) (**D**) Capsule size measured after India

1315 ink staining was significantly larger in titan cells (TC) than in typical cells (tC) both *in vitro* and

1316 *in vivo*, in general, the capsule was larger *in vivo* independently of the cell size (p<0.0001).

1317 Dots represent individual cells, and boxes median and IQR for 250 cells each (*p<0.001); (**E**).

1318 The budding rate of titan cells was lower compared to that of typical cells upon incubation in

1319 minimal medium (MM) after titan cells generation *in vitro* *(p=0.018) but not *in vivo*. *In vivo*,

1320 budding rate of titan cells (TC) and typical cells (tC) were equivalent and increased as

1321 compared to *in vitro* titan cells and typical cells and controls (**p<0.001).(**F**) The yeasts

1322 recovered at step 4 of the protocol and analyzed by dot plots (FSC/SSC) using flow cytometry

1323 included two populations FSC/SSC^{high} and FSC/SSC^{low} representing titan cells (TC) and typical

1324 cells (tC), respectively; (**G**) DNA content analysis after propidium iodide (PI) staining showed

1325 that the titan cells (FSC/SSC^{high}) population harbored increased PI fluorescence intensity from

1326 2C to >4C (red arrow) as compared to the diploid control (AD7-77 cultured in Sabouraud agar)
1327 while the typical cells (FSC/SSC^{low}) population harbored a PI intensity comparable to the
1328 haploid control (H99O cultured in Sabouraud agar).
1329
1330 **Fig 2. Titan cells harbor an increased chitin content and a specific capsule structure *in vitro***
1331 **and *in vivo* using multispectral imaging flow cytometry.**
1332 (**A**) Titan cells (TC) and typical cells (tC) were selected in the corresponding gates based on the
1333 Area/Diameter dot plot. **(B)** Titan cells *in vivo* are bigger than that produced *in vitro*. The chitin
1334 content based on calcofluor white (CFW) fluorescence intensity showed significantly increased
1335 fluorescence of titan cells compared to typical cells *in vitro* (**C**) and *in vivo* (**D**). Based on the
1336 fluorescence pattern of the 2D10 anti-capsular monoclonal antibody, the algorithms
1337 "modulation" and "bright details intensity R7" allowed to discriminate the capsule structure
1338 of titan cells and typical cells with almost no overlap between both population *in vitro* (**E**) and
1339 *in vivo* (**F**).
1340
1341 **Fig 3**. **Dynamics of titan cells generation *in vitro***.
1342 (**A**) Cell body size was measured from samples of H99O culture (step 3 of the protocol)
1343 withdrawn at specific times (H0 to H120) using pictures taken in bright field and measured
1344 with the ICY software (mean number of yeasts counted ± SD = 219 ± 67, representative of
1345 three experiments). Cell size increased starting at H8 with some cells reaching the threshold
1346 of 10 µm (grey dashed line). Each dot represents a single cell and the bars represent median
1347 and IQR; (**B**) Titan cells generation started between H8 and H12 and reached a plateau at H24.
1348 Each dot represents the proportion of titan cells in the corresponding sample (3 independent
1349 experiments); (**C**) Pictures (x400 magnification) taken overtime showing the progressive

1350 increase in cell body size and the appearance of a vacuole typical of titan cells in a large cell at
1351 H8 (white arrow) (scale bar 10 µm); (**D**) Time lapse imaging of titan cells generation over 12 h
1352 showing that titan cells swelled progressively from a small cell and produced daughter cells
1353 after having increased their size. (**E**) Cells stained with calcofluor (CFW) at 0.1 µg/mL prior to
1354 incubation using our protocol. CFW fluorescent intensity is analyzed by flow cytometry in the
1355 initial (H0) and the resulting FSC/SSC^{high} (titan cells) and FSC/SSC^{low} (typical cells) observed at
1356 H24. The initial (H0) (green line) and the H24 FSC/SSC^{high} (blue line) populations harbored a
1357 high CFW fluorescence suggesting that they are mother cells, with a higher fluorescence for
1358 the FSC/SSC^{high}, while two populations of high and low (black star) CFW fluorescence intensity
1359 were observed for the H24 FSC/SSC^{low} cells (Left panel). The right panel shows the size (FSC)
1360 and CFW fluorescence intensity of the yeast populations at H0 (black content lines) and H24
1361 (yellow content lines). The initial population (CFW^{high}/FSC^{low}) evolved in two populations, one
1362 corresponding to daughter cells (typical cells, CFW^{low}/FSC^{low}, white arrow), and the other one
1363 corresponding to titan cells (CFW^{high}/FSC^{high}, black arrow).
1364
1365 **Fig 4. Titan cells generation *in vitro* is impacted by various environmental conditions**.
1366 (**A**) The sequence of media used at steps 2 and 3 of the protocol was crucial for titan cells
1367 generation: yeasts cultured in Yeast Peptone Dextrose (YPD) and transferred to minimal
1368 medium (MM) produced significantly more titan cells (cells >10µm, dotted grey line) than
1369 yeasts cultured in MM or YPD and transferred in MM or YPD, respectively; (**B**) Exposure to d
1370 light at step 3 had a positive impact on titan cells generation compared to incubation in the
1371 dark; (**C**) Raising the incubation temperature to 37°C at step 3 decreased titan cells formation
1372 compared to 30°C; (**D**) Modification of the initial pH of the MM used at step 3 modifies titan
1373 cells formation with pH 5.5 being optimal while a more acidic (pH=4), a neutral (pH=7) or an

1374 alkaline (pH=8.5) pH inhibited titan cells formation; (**E**) The impact of hypoxia was tested by
1375 physical (closed cap) and by chemical ($COCl_2$ in MM at 1 nM) method and compared to
1376 normoxia (21% oxygen). Physically- and chemically-induced hypoxia enhances the production
1377 of titan cells compared to normoxia with a higher proportion of titan cells in chemically-
1378 compared to physically-induced hypoxia. All experiments were performed in triplicate and
1379 pooled (mean cell counted ± SD =2305±1438). Median and IQR are shown in black for each
1380 condition (* $p<0.0001$ vs reference condition). The percentages above each condition
1381 represents the % of titan cells observed.

1382

1383 **Fig 5. Titan cells generation *in vitro* is influenced *in vitro* by host derived cues and ergosterol,**
1384 **protein and RNA inhibitors.**

1385 (**A**) Monoclonal anti-cryptococcal capsular polysaccharide antibodies E1 and 18B7 (at 166
1386 µg/mL in MM) significantly decreased cell size, as fetal calf serum (FCS, 5%) (**B**) and
1387 phosphatidylcholine at 5mM (**C**) did. (**D**) Fluconazole ; (**E**) flucytosine at concentration below
1388 the MIC (4 mg/L) and (**F**) cycloheximide at 0.1µg/mL drastically impaired titan cells formation
1389 with almost no titan cells produced upon drug exposure.

1390

1391 **Fig 6. Generation of titan cells *in vitro* is influenced by cell concentration and quorum sensing**
1392 **molecules.**

1393 (**A**) The cell concentration at onset of step 2 significantly modified titan cells generation with
1394 a maximal titan cells formation using an initial concentration of 10^6 cells/mL, and an abolition
1395 of titan cells formation at 10^7 cells/mL; We then tested several factors at step 3 by adding (**B**)
1396 Pantothenic acid (PA) at 125 µM which had no impact on cell size distribution but significantly
1397 increased the proportion of titan cells produced; (**C**) quorum sensing peptide 1 (Qsp1p, 10µM)

1398 which significantly decreased cell size distribution and the proportion of titan cells produced;
1399 (**D**) The proportion of titan cells generated is influenced by the concentration of PA with a
1400 significant increase of titan cells at 0.125 µM and 12.5 µM (* p<0.001). (**E**) Growth curves were
1401 measured continuously during titan cells generation and showed a significant increase of the
1402 doubling time (slope) from 0.125 µM of PA on. titan cells formation and growth rate is not
1403 correlated since titan cells formation is inhibited at 1250 µM of PA and the doubling time
1404 increased. (**F**) Qsp1 acts as a repressor of titan cells formation as the addition of Qsp1 peptide
1405 inhibited titan cells formation (*p<0.001). A control using scrambled peptide showed no effect
1406 on titan cells formation. The *qsp1Δ* and *pqp1Δ* complemented by addition of Qsp1p showed
1407 an increase in titan cells formation. No effect of the Qsp1p was observed on *opt1Δ*, the
1408 deletion mutant of the Qsp1 transporter Opt1. A specific titan cells inducing conditions was
1409 implemented for D, E, and F to allow induction of titan cells in a 100-well plate and continuous
1410 measurements of growth curves using the Bioscreen apparatus.
1411
1412 **Fig 7. Titan cells generation is dependent on various genes and requires signaling through**
1413 **the Gpr/PKA/Rim101 pathway *in vitro*.**
1414 (**A**) The different H99 strains harbored variable abilities to produce titan cells compared to
1415 H99O (grey bar) with high titan cells producer (H99O, S, L) and low titan cells producer (KN99α,
1416 H99W, H99 CMO18) *in vitro*. (**B)** *Sgf29Δ* and *lmp1Δ* deletion mutants show a decrease in titan
1417 cells generation in various H99 backgrounds *in vitro* compared to H99O. Complementation in
1418 strains *lmp1Δ:LMP1* and *sgf29Δ:SGF29* in H99S background restored the phenotype of H99S.
1419 Rim101 (**C**) and *GPR4* and *GPR5* and *CAC1* **(D)** are required for titan cells generation *in vitro* in
1420 H99 and KN99α. The ratio to the value obtained for H99O used as a calibrator in each
1421 experiment was calculated for each strain. Bar represent mean ± SD (mean cell counted=600).

1422 Khi2 test was performed to compare the experimental conditions to H99O, they were
1423 performed in triplicates and pooled (*p<0.0001, **p<0.0001, when the comparison was done
1424 with the parental strain H99S.)
1425
1426 **Fig 8. Non-synonymous mutation of *PKR1* enhances titan cells generation based on clinical**
1427 **isolates analysis.**
1428 (**A**) The screening of 56 *C. neoformans* serotype A MATα french clinical isolates identified
1429 isolates AD2-06a (ratio=2.6±0.2) and AD2-02a (ratio=1.4±0.2) as titan cells producers
1430 compared to H99O (grey bar); (**B**) Phylogenic tree of the isolates (n=41) for which the whole
1431 sequence was available [38,39] was estimated using RAxML under the GTRCAT model. This
1432 shows that AD2-06a, AD2-07 and AD3-55a are phylogenetically close together. (**C**) Venn
1433 diagram representing the number of common or specific SNPs and Indel between AD2-06a,
1434 AD2-07 and AD3-55a. One of the four AD2-06a specific SNPs is a non-synonymous mutation
1435 in the *PKR1* gene (mutation Gly125fs); (**D**) Alignment of Pkr1 protein sequences from selected
1436 clinical isolates including H99O and AD2-07 that both harbor a wild type sequence. The Pkr1
1437 domain architecture is formed by a dimerization domain in green (amino acids 2 to 40) and
1438 two cAMP binding sites based on INTERPRO model in red (amino acids 219 to 351 and 353 to
1439 473). (**E**) Strains with *PKR1* loss-of-function mutation showed a variable ability to produce titan
1440 cells, as compared to H99O (grey bar). The clinical isolate AD2-07, which produces significantly
1441 less titan cells was recovered from the CSF of an HIV-positive patient on d 13 of amphotericin
1442 B treatment while AD2-06a, which produced the highest proportion of titan cells, was
1443 recovered from the initial CSF sample of the same patient. (**F**) Complementation of *PKR1* gene
1444 (*AD2-06a:PKR1*) in the naturally deficient strain AD2-06a reduced titan cells generation
1445 compared to AD2-06a. The ratio to H99O, used as a calibrator in each experiment, was

1446 calculated for each strain (panel A, E, F) and results expressed as mean ±SD. Experiments A, F
1447 and G were done in triplicate, B twice (screening). To compare the experimental conditions to
1448 H99O, Khi2 analysis was performed (*p<0.0001, **p<0.05). Mean cell counted ± SD =
1449 1165±528.
1450
1451 **Fig 9. *In vitro* titan cells generation is dependent on the negative regulator *PKR1* and *TSP2*.**
1452 **(A)** *PKR1* is a repressor of titan cells formation in KN99α background and (**B**) in H99
1453 background. (**C**) in galactose mimimal medium (galactose MM), GAL7 promoter upstream of
1454 the *PKA1* and *PKR1* genes induced an increased titan cells formation for PKA1 and a decreased
1455 titan cells formation for PKR1 (**D**) In minimal medium with glucose (glucose MM)), GAL7
1456 promoter induced a repression of titan cells formation for PKA1 and an induction of titan cells
1457 formation for PKR1. (**E**) Tetraspanin 2 (*TSP2*) is a repressor of titan cells formation.
1458 Complementation of the deletion mutants restored the phenotype of KN99α. The ratio to H99
1459 or KN99α, used as a calibrator in each experiment, was calculated for each strain (panel A to
1460 E) and results expressed as mean ± SD. Experiments A to G were done in triplicate. To compare
1461 the experimental conditions to H99O, Khi2 analysis was performed (*p<0.0001 vs control H99
1462 or KN99α or appropriate mutants)

1463 **Table 1: Genes affected by SNPs or Indels in the different H99 strains**

1464

Strains	Genes affected	Gene function	Genetic event
H99O	*CNAG_07634*	hypothetical	Deletion
	CNAG_04078	hypothetical	Insertion
	CNAG_06456	hypothetical	Insertion
H99S	*CNAG_07595*	hypothetical	Deletion/frameshift
	CNAG_12447	miscRNA	Insertion
	CNAG_12900	miscRNA	Insertion
H99L	CNAG_06392, *SGF29*	transcription factor (binds H3K4me2/3 and recruits histone deacetylation)	Deletion
KN99α	CNAG_06392, *SGF29*	transcription factor (binds H3K4me2/3 and recruits histone deacetylation)	Deletion
H99W	*CNAG_06765*, *LMP1*	Hypothetical (involved in mating virulence and melanization)	Deletion/frameshift
H99 CMO18	*CNAG_06765*, *LMP1*	Hypothetical (involved in mating virulence and melanization)	Deletion/frameshift

1465

1466

1467 **Table 2 – Alignment and SNP statistics of sequenced isolates using H99 as a reference.**

1468

Strain	MLST genotype	% of Assembly Covered by aligned reads	Alignment depth (X)	SNPs
AD3-55a	unique	100	133	28,070
AD2-06a	unique	100	129	28,202
AD2-07	unique	99	45	27,797
AD3-41a	unique	100	134	25,378
AD4-92a	A3/M3	100	132	11,906
AD4-47a	A4/M1	100	132	10,018
AD3-58	A4/M1	100	123	9,996
AD3-83a	A1/M1	100	166	172
AD2-99a	A1/M1	100	119	180
AD6-55a	related to A1/M1	100	108	12,440
AD6-54a	related to A1/M1	100	131	12,440
AD5-45a	related to A1/M1	100	142	12,417
AD1-95a	related to A1/M1	100	107	12,521
AD1-90a	related to A1/M1	100	122	12,511
AD5-67a	VNII	100	139	277,381
AD3-9a	VNII	100	111	277,417
AD3-11a	VNII	100	125	268,842
AD4-76a	Th	100	112	43,281
AD3-95a	Th	100	141	43,235
AD5-53a	A5/M5	100	130	42,291
AD2-82a	A5/M5	100	133	42,271
AD1-86a	A5/M5	100	105	43,778
AD5-39a	A4/M4	100	108	43,696
AD4-63a	A4/M4	100	129	43,736
AD2-04a	A4/M4	100	137	43,733
AD1-68a	A4/M4	100	132	43,778

1469

1470

1471 **Table 3: Mutations of *PKR1*, *CAC1*, *USV101* in specific clinical isolates**

1472

Gene	Strains	Mutations
PKR1	Ug2462	n.1333C>T|p.Arg445*|1333/1449
	Bt117	n.1274_1280dupCTCTCCT|p.Asn428fs|1280/1449
	Bt77	n.1293dupA|p.Arg432fs|1293/1449
	8-1	n.878_911delCCGAGGGGAGCTCGTTTGGGGAGTTAGCGCTGAT|p.Ser293fs|911/1449
	Bt58	n.742G>T|p.Glu248*|742/1449
	AD2-06a	n.375_376delAG|p.Gly125fs|376/1449
	Bt156	n.41dupA|p.Asp14fs|41/1449
CAC1	Bt133	n.41delA|p.His14fs |41/6930
	8-1	n.2_3insA| |p.Met1fs|2/6930 ; n.80G>A|p.Trp27*|80/6930 ; n.81G>A|p.Trp27*|81/6930
	AD3-11a	n.2_3insA| |p.Met1fs|2/6930
	AD3-9a	n.2_3insA| |p.Met1fs|2/6930
	AD5-67a	n.2_3insA| |p.Met1fs|2/6930
	Ug2462	n.2_3insA| |p.Met1fs|2/6930
USV101	Bt88	n.842dupC|p.His282fs

1473 *, stop codon introduced by the SNP

1474

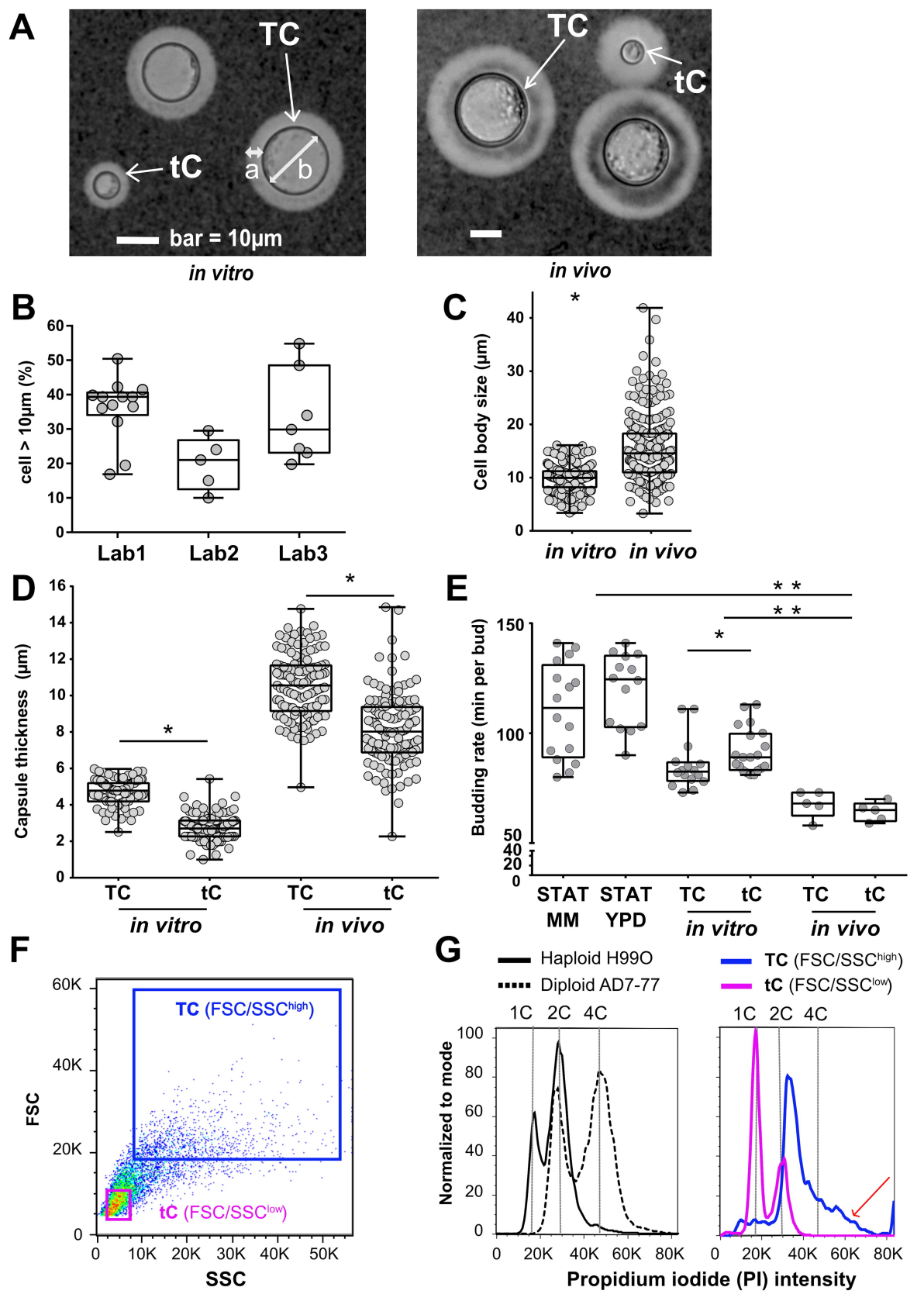
A
TC
tC
a
b
bar = 10µm
in vitro
TC
tC
in vivo
B
cell > 10µm (%)
Lab1
Lab2
Lab3
C
Cell body size (µm)
in vitro
in vivo
D
Capsule thickness (µm)
TC
tC
TC
tC
in vitro
in vivo
E
Budding rate (min per bud)
STAT MM
STAT YPD
TC
tC
TC
tC
in vitro
in vivo
F
FSC
SSC
TC (FSC/SSC^high)
tC (FSC/SSC^low)
G
Haploid H99O
Diploid AD7-77
TC (FSC/SSC^high)
tC (FSC/SSC^low)
1C 2C 4C
Normalized to mode
Propidium iodide (PI) intensity

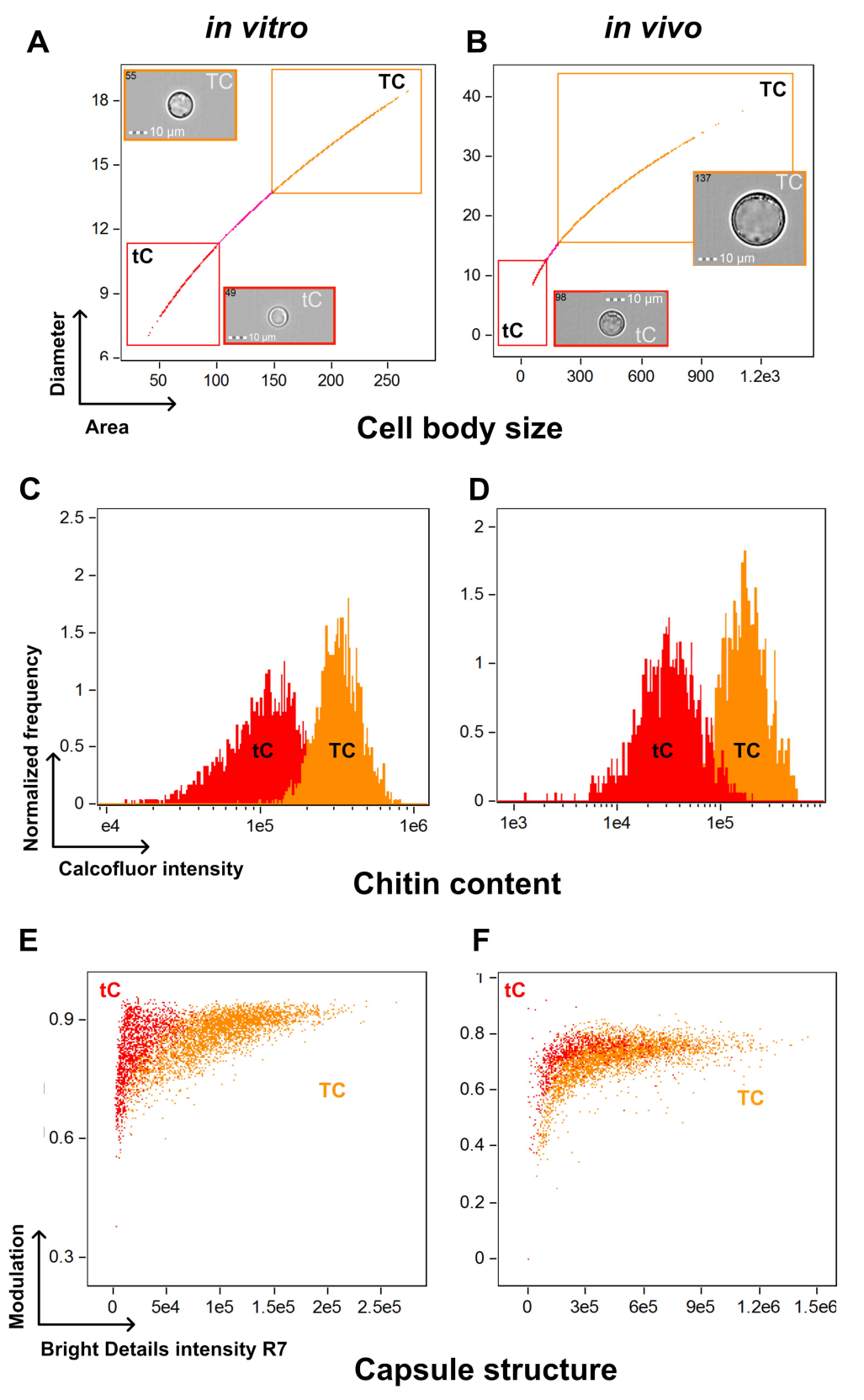
A
in vitro
B
in vivo
TC
tC
10 µm
Diameter
Area
Cell body size
C
D
Normalized frequency
Calcofluor intensity
Chitin content
E
F
Modulation
Bright Details intensity R7
Capsule structure

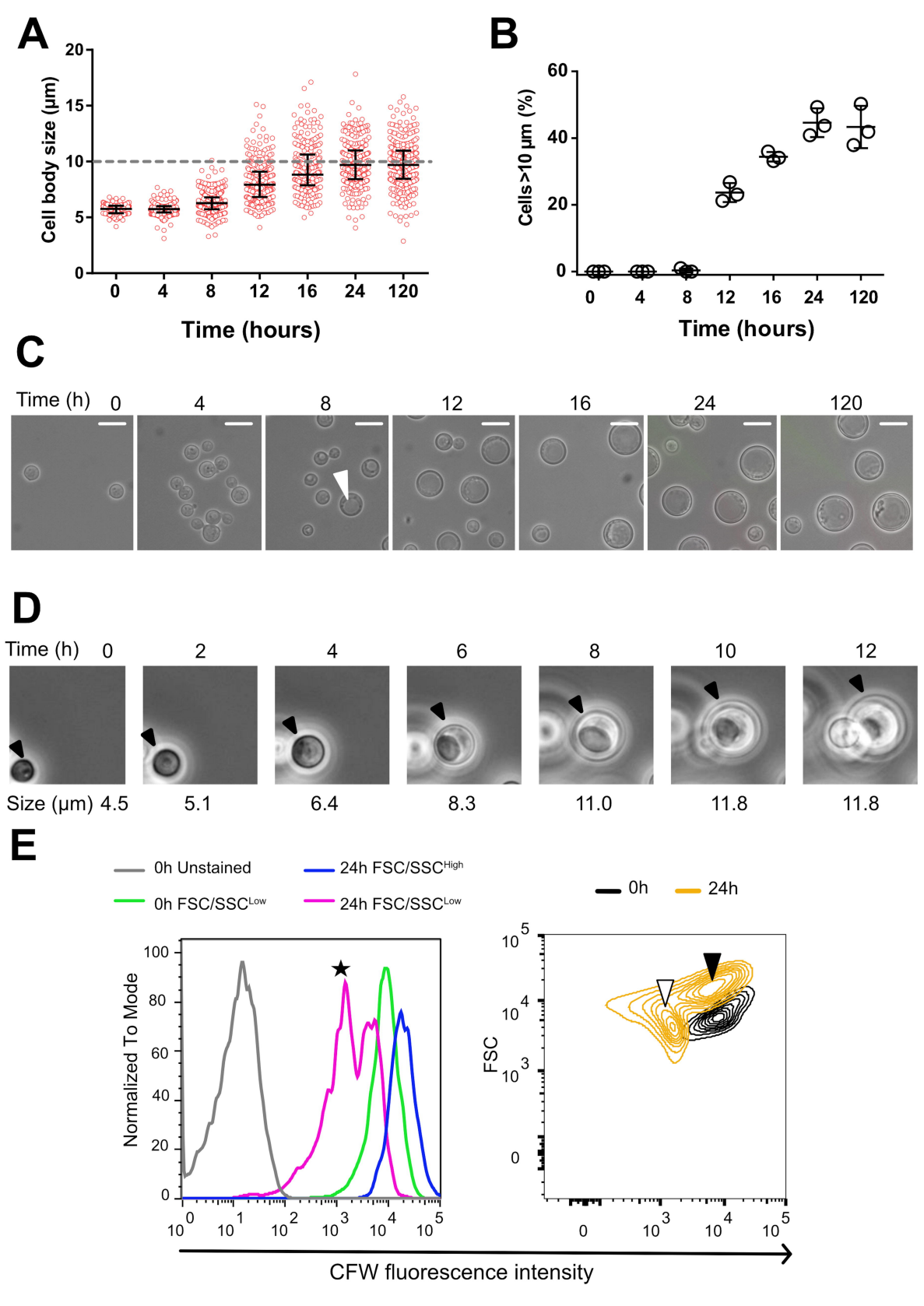
A
Cell body size (µm)
Time (hours)
B
Cells>10 µm (%)
Time (hours)
C
Time (h)
0
4
8
12
16
24
120
D
Time (h)
0
2
4
6
8
10
12
Size (µm)
4.5
5.1
6.4
8.3
11.0
11.8
11.8
E
0h Unstained
0h FSC/SSC^Low
24h FSC/SSC^High
24h FSC/SSC^Low
Normalized To Mode
0h
24h
FSC
CFW fluorescence intensity

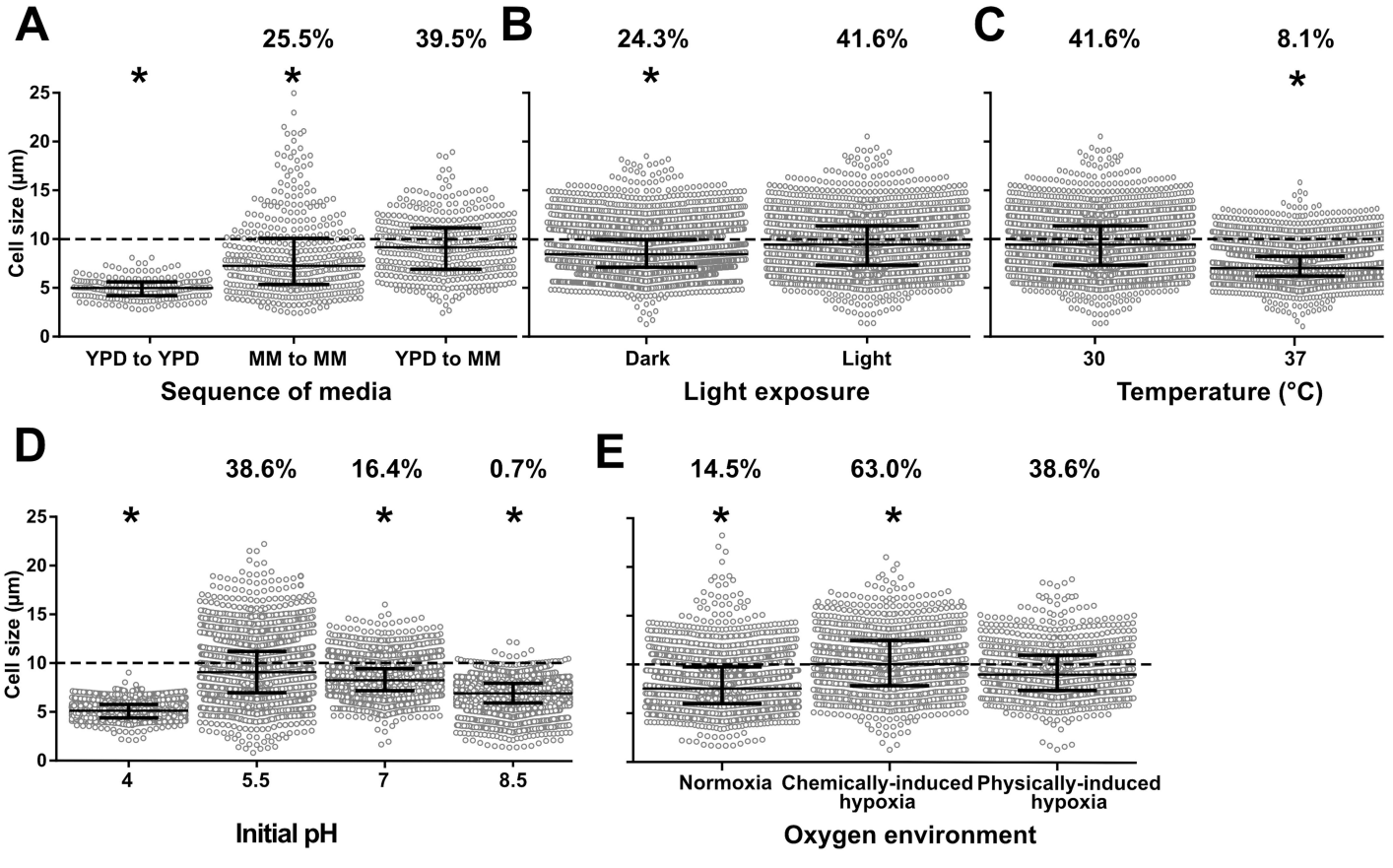
A
25.5%
39.5%
*
*
Cell size (µm)
25
20
15
10
5
0
YPD to YPD
MM to MM
YPD to MM
Sequence of media
B
24.3%
41.6%
*
Dark
Light
Light exposure
C
41.6%
8.1%
*
30
37
Temperature (°C)
D
38.6%
16.4%
0.7%
*
*
*
Cell size (µm)
25
20
15
10
5
0
4
5.5
7
8.5
Initial pH
E
14.5%
63.0%
38.6%
*
*
Normoxia
Chemically-induced hypoxia
Physically-induced hypoxia
Oxygen environment

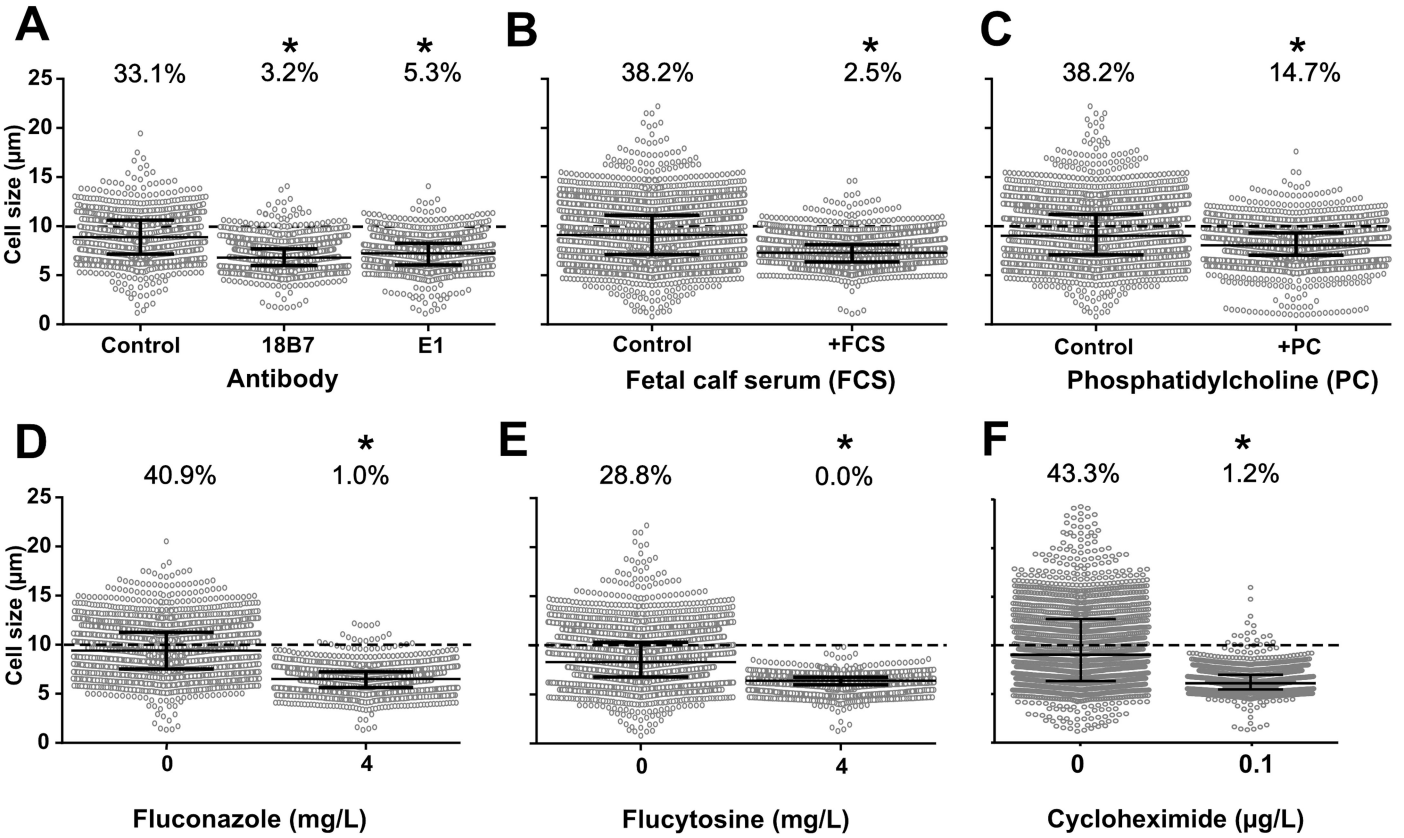
A
33.1%
*
3.2%
*
5.3%
Cell size (µm)
25
20
15
10
5
0
Control
18B7
E1
Antibody
B
38.2%
*
2.5%
Control
+FCS
Fetal calf serum (FCS)
C
38.2%
*
14.7%
Control
+PC
Phosphatidylcholine (PC)
D
40.9%
*
1.0%
Cell size (µm)
25
20
15
10
5
0
0
4
Fluconazole (mg/L)
E
28.8%
*
0.0%
0
4
Flucytosine (mg/L)
F
43.3%
*
1.2%
0
0.1
Cycloheximide (µg/L)

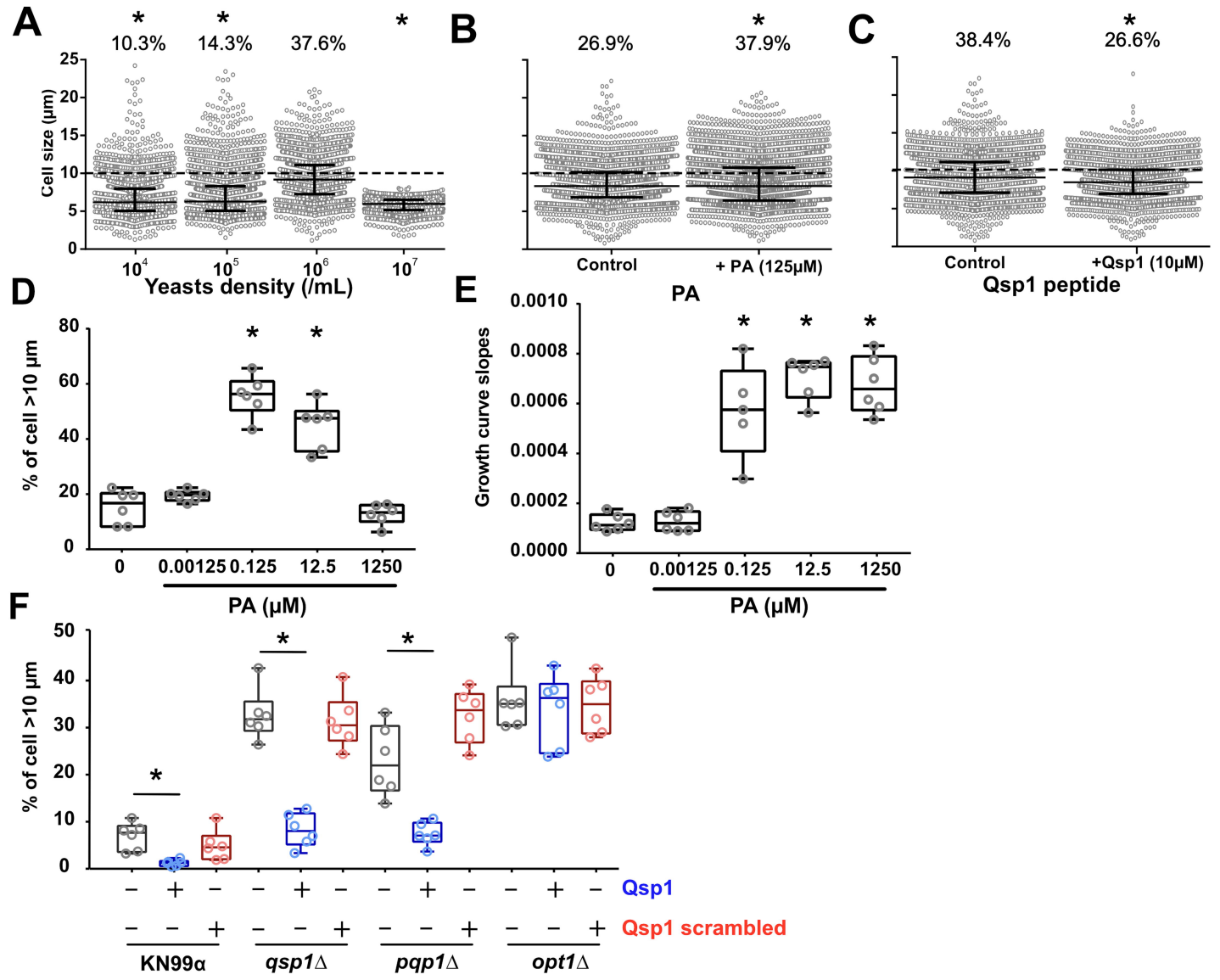
A
10.3%
14.3%
37.6%
Cell size (µm)
Yeasts density (/mL)
B
26.9%
37.9%
Control
+ PA (125µM)
C
38.4%
26.6%
Control
+Qsp1 (10µM)
Qsp1 peptide
D
% of cell >10 µm
PA (µM)
E
PA
Growth curve slopes
PA (µM)
F
% of cell >10 µm
Qsp1
Qsp1 scrambled
KN99α
qsp1Δ
pqp1Δ
opt1Δ

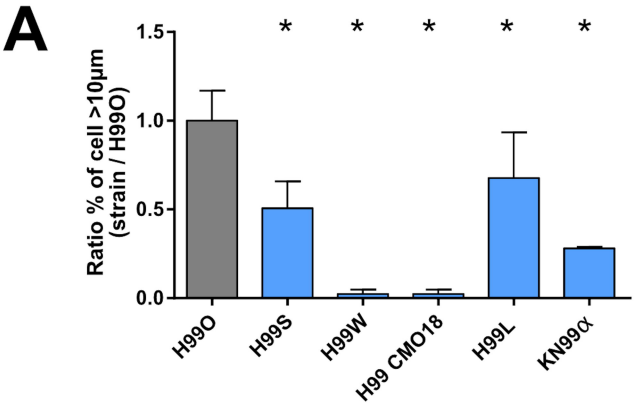
A
Ratio % of cell >10µm
(strain / H99O)
1.5
1.0
0.5
0.0
*
*
*
*
*
H99O
H99S
H99W
H99 CMO18
H99L
KN99α

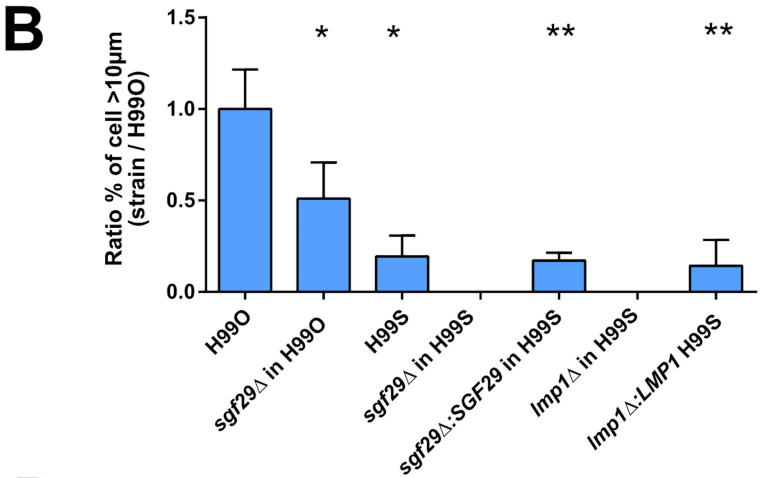
B
Ratio % of cell >10µm
(strain / H99O)
1.5
1.0
0.5
0.0
*
*
**
**
H99O
sgf29Δ in H99O
H99S
sgf29Δ in H99S
sgf29Δ:SGF29 in H99S
lmp1Δ in H99S
lmp1Δ:LMP1 H99S

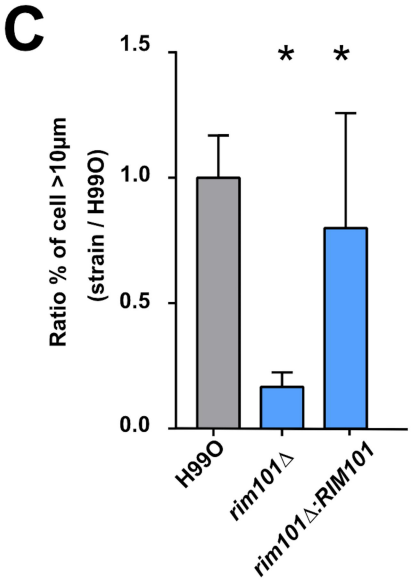
C
Ratio % of cell >10µm
(strain / H99O)
1.5
1.0
0.5
0.0
*
*
H99O
rim101Δ
rim101Δ:RIM101

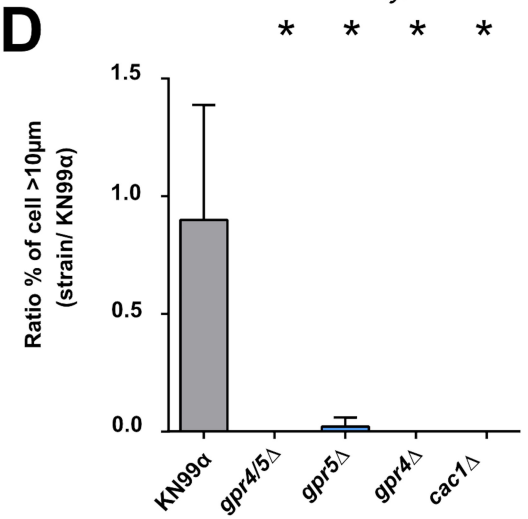
D
Ratio % of cell >10µm
(strain/ KN99α)
1.5
1.0
0.5
0.0
*
*
*
*
KN99α
gpr4/5Δ
gpr5Δ
gpr4Δ
cac1Δ

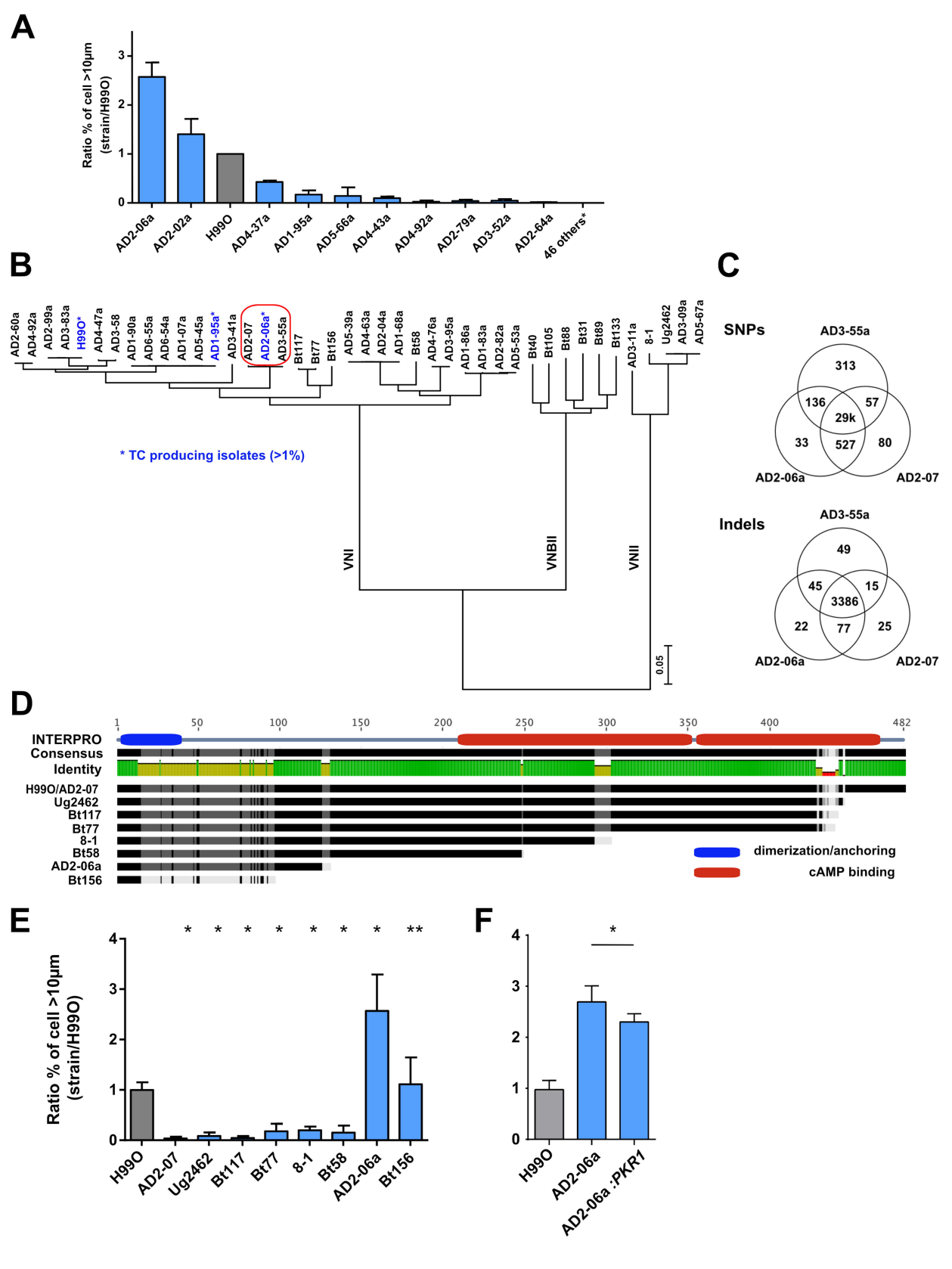
A
Ratio % of cell >10µm (strain/H99O)
AD2-06a
AD2-02a
H99O
AD4-37a
AD1-95a
AD5-66a
AD4-43a
AD4-92a
AD2-79a
AD3-52a
AD2-64a
46 others*
B
AD2-60a
AD4-92a
AD2-99a
AD3-83a
H99O*
AD4-47a
AD3-58
AD1-90a
AD6-55a
AD6-54a
AD1-07a
AD5-45a
AD1-95a*
AD3-41a
AD2-07
AD2-06a*
AD3-55a
Bt117
Bt77
Bt156
AD5-39a
AD4-63a
AD2-04a
AD1-68a
Bt58
AD4-76a
AD3-95a
AD1-86a
AD1-83a
AD2-82a
AD5-53a
Bt40
Bt105
Bt88
Bt31
Bt89
Bt133
AD3-11a
8-1
Ug2462
AD3-09a
AD5-67a
* TC producing isolates (>1%)
VNI
VNBII
VNII
0.05
C
SNPs
AD3-55a
313
136
57
29k
33
527
80
AD2-06a
AD2-07
Indels
AD3-55a
49
45
15
3386
22
77
25
AD2-06a
AD2-07
D
1
50
100
150
200
250
300
350
400
482
INTERPRO
Consensus
Identity
H99O/AD2-07
Ug2462
Bt117
Bt77
8-1
Bt58
AD2-06a
Bt156
dimerization/anchoring
cAMP binding
E
Ratio % of cell >10µm (strain/H99O)
H99O
AD2-07
Ug2462
Bt117
Bt77
8-1
Bt58
AD2-06a
Bt156
F
H99O
AD2-06a
AD2-06a :PKR1

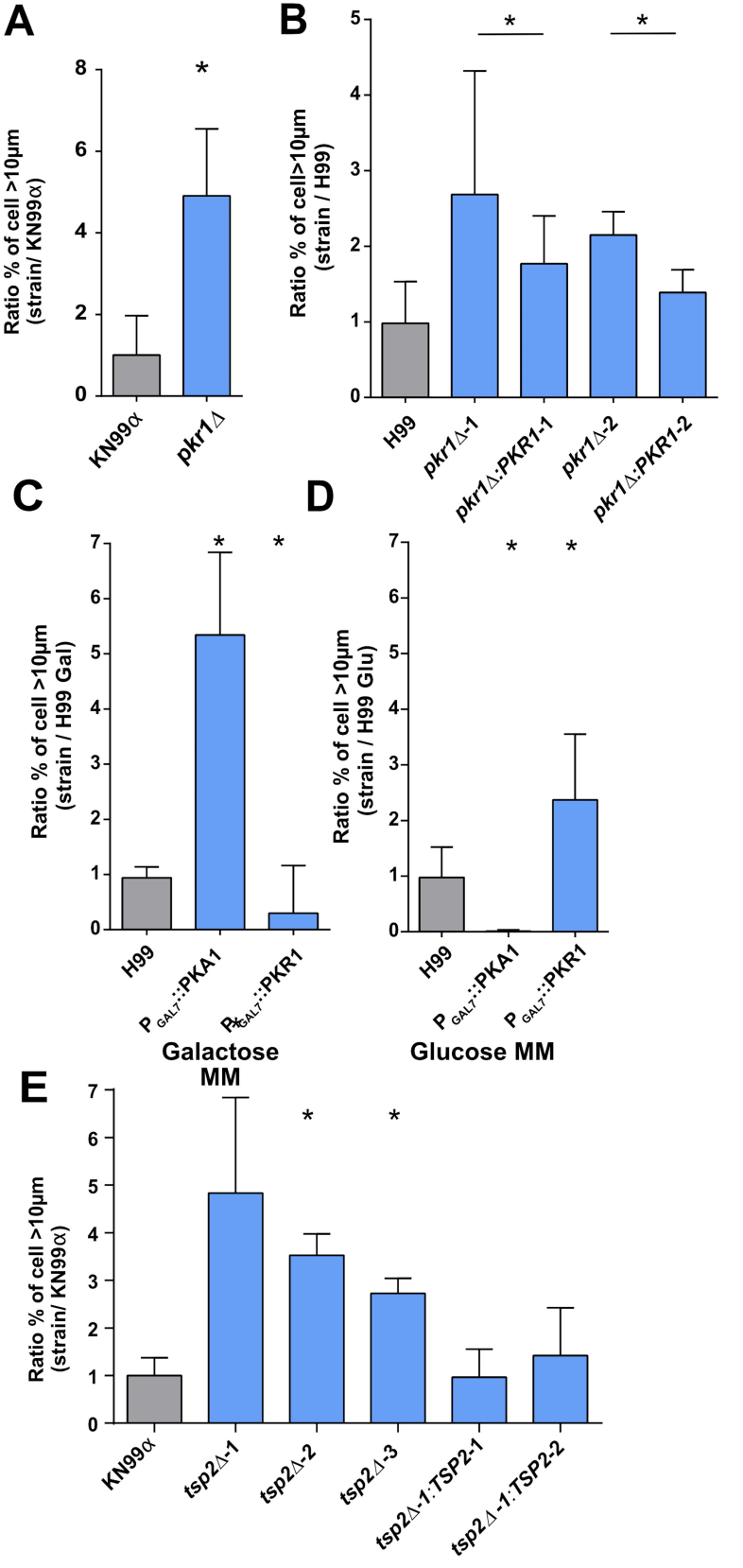
A
Ratio % of cell >10µm (strain/ KN99α)
KN99α
pkr1Δ
B
Ratio % of cell>10µm (strain / H99)
H99
pkr1Δ-1
pkr1Δ:PKR1-1
pkr1Δ-2
pkr1Δ:PKR1-2
C
Ratio % of cell >10µm (strain / H99 Gal)
H99
P GAL7::PKA1
P GAL7::PKR1
Galactose MM
D
Ratio % of cell >10µm (strain / H99 Glu)
H99
P GAL7::PKA1
P GAL7::PKR1
Glucose MM
E
Ratio % of cell >10µm (strain/ KN99α)
KN99α
tsp2Δ-1
tsp2Δ-2
tsp2Δ-3
tsp2Δ-1:TSP2-1
tsp2Δ-1:TSP2-2